The ubiquitin-like modifier FAT10 inhibits retinal PDE6 activity and mediates its proteasomal degradation

Annika N. Boehm[1,2], Johanna Bialas[1,2], Nicola Catone[2], Almudena Sacristan-Reviriego[3], Jacqueline van der Spuy[3], Marcus Groettrup[1,2] , and Annette Aichem[1,2,]*

From the [1]Division of Immunology, Department of Biology, University of Konstanz, Konstanz, Germany, the [2]Biotechnology Institute Thurgau at the University of Konstanz, Kreuzlingen, Switzerland, and the [3]UCL Institute of Ophthalmology, University College London, London, United Kingdom

Edited by George N. DeMartino

The retina-specific chaperone aryl hydrocarbon interacting protein-like 1 (AIPL1) is essential for the correct assembly of phosphodiesterase 6 (PDE6), which is a pivotal effector enzyme for phototransduction and vision because it hydrolyzes cGMP. AIPL1 interacts with the cytokine-inducible ubiquitin-like modifier FAT10, which gets covalently conjugated to hundreds of proteins and targets its conjugation substrates for proteasomal degradation, but whether FAT10 affects PDE6 function or turnover is unknown. Here, we show that FAT10 mRNA is expressed in human retina and identify rod PDE6 as a retina-specific substrate of FAT10 conjugation. We found that AIPL1 stabilizes the FAT10 monomer and the PDE6-FAT10 conjugate. Additionally, we elucidated the functional consequences of PDE6 FAT10ylation. On the one hand, we demonstrate that FAT10 targets PDE6 for proteasomal degradation by formation of a covalent isopeptide linkage. On the other hand, FAT10 inhibits PDE6 cGMP hydrolyzing activity by noncovalently interacting with the PDE6 GAFa and catalytic domains. Therefore, FAT10 may contribute to loss of PDE6 and, as a consequence, degeneration of retinal cells in eye diseases linked to inflammation and inherited blindness-causing mutations in AIPL1.

The process of vision is very complex and needs to be tightly controlled. Because retinal cells, especially the rod and cone photoreceptors, have an unusually high demand for the synthesis and thus folding of proteins involved in phototransduction, a specialized chaperone machinery is needed to guarantee retinal proteostasis (1–4). One member of this machinery is the aryl hydrocarbon interacting protein-like 1 (AIPL1), which together with Hsp70 and Hsp90 forms a chaperone heterocomplex (5). AIPL1 is exclusively expressed in developing photoreceptors, adult rods, and the pineal gland (6–8). Its importance becomes apparent because even point mutations within the *Aipl1* gene, such as A197P or C239R, induce an inherited retinal degenerative disease called Leber congenital amaurosis (LCA), which is characterized by the loss of vision during the first months of life (6, 9).

Within photoreceptors, AIPL1 is important for chaperoning retinal phosphodiesterase 6 (PDE6) (3). AIPL1 was not only shown to interact with PDE6 but also to be essential for the proper assembly of PDE6 subunits into a holoenzyme (10). Within rods and cones, PDE6 differs in the composition of the catalytic core. Whereas rod PDE6 possesses a heterodimeric catalytic core consisting of an α- and a β-subunit, cone PDE6 is composed of two catalytic α′-subunits. Nonetheless, both interact with two photoreceptor-specific inhibitory γ-subunits (11–13). Just like other PDE superfamily members, the PDE6 catalytic subunits harbor two N-terminal regulatory GAF domains and a C-terminal catalytic domain (14–16). PDE6 is one of the key enzymes of phototransduction. Briefly, after activation of a visual pigment, the G protein transducin is activated, leading to the interaction of the activated transducin α-subunit with the PDE6 γ-subunits. This leads to an increased and accelerated PDE6-mediated cGMP hydrolysis resulting in a drop of intracellular cGMP levels. Subsequently cGMP-gated ion channels are closed and the photoreceptor membrane is hyperpolarized, resulting in a synaptic transmission of the signal (2, 17, 18). This whole phototransduction process takes place in the outer segment of photoreceptors where PDE6 is anchored in membrane disks via posttranslational prenylation of the catalytic subunits (19, 20).

We have recently published another interaction partner of AIPL1, human leukocyte antigen (HLA)-F adjacent transcript 10 (FAT10) protein (21). FAT10 belongs to the family of ubiquitin-like modifiers and is, in contrast to the ubiquitously expressed ubiquitin, constitutively expressed only in organs and unique cell types of the immune system (22–25). In other cell types, FAT10 is expressed upon synergistic induction by the pro-inflammatory cytokines tumor necrosis factor (TNF)α and IFN-γ (26, 27). The 18-kDa FAT10 protein consists of two ubiquitin-like domains (UBD) bearing the typical ubiquitin β-grasp fold, whereas the C-terminal domain contains the diglycine motif important for covalent attachment to substrates (28, 29). This conjugation is mediated by an enzyme cascade consisting of the E1 activating enzyme UBA6 (30–32), the E2 conjugating enzyme USE1 (26, 33), and putative E3 ligases. FAT10ylation of conjugation substrate proteins such as USE1 itself (26), the autophagy receptor p62 (34), or the ubiquitin-activating enzyme UBE1 (35), targets them directly for proteasomal degradation. Of note, this is independent of additional ubiquitin attachment or the activity of the segregase valosin-containing protein (VCP) (28, 36–38). Next to covalent modification of substrates, FAT10 can also interact with proteins in a noncovalent manner, resulting, for example, in an altered

functionality of the interaction partner, as recently shown for the deubiquitinating enzyme OTUB1 (39) or for the SUMO E1 activating enzyme AOS1/UBA2 (40).

In this study, we examined the specific function of FAT10 in photoreceptor cells, inspired by the recently identified interaction between AIPL1 and FAT10. We present evidence that FAT10 expression is inducible in human retinal cells, and we identify PDE6 as the first retina-specific FAT10 conjugation substrate. By investigating the impact of AIPL1 on FAT10 and the FAT10-PDE6β conjugate, we show that both accumulate in the presence of AIPL1. Finally, we examined the functional consequences and show that the modification of PDE6 by covalent attachment of FAT10 targets PDE6 for proteasomal degradation, whereas noncovalent interaction with FAT10 downregulates the enzymatic activity of PDE6.

Results

FAT10 interacts via both UBL domains with the tetratricopeptide repeat motifs in AIPL1

We have recently reported that the retinal chaperone AIPL1 interacts with the ubiquitin-like modifier FAT10 (21). We first aimed to further confirm this finding with endogenous FAT10 *in cellulo* (Fig. 1A). For this purpose, we overexpressed myc-tagged WT AIPL1 (myc-AIPL1) and AIPL1 mutants known to cause LCA (myc-AIPL-A197P and myc-AIPL1-C239R) in HEK293 cells and induced endogenous FAT10 expression by stimulation with the pro-inflammatory cytokines TNFα and IFN-γ. Subsequent co-immunoprecipitation (Co-IP) confirmed an interaction of endogenous FAT10 with all three AIPL1 variants (Fig. 1A, lanes 6–8). Because AIPL1-A197P and AIPL1-C239R interacted with FAT10, we tested further pathogenic AIPL1 mutants for a possible interaction with FAT10 under overexpression conditions (Fig. S1, A and B). Interestingly, we found that all tested AIPL1 mutants (AIPL1-R38C, -W72S, -C89R, -A197P, -C239R, -G262S, and -P376S) interacted with FAT10, indicating that the point mutations do not affect AIPL1 concerning its ability to interact with FAT10.

Because AIPL1 WT had been shown to interact with FAT10 in a direct manner (21), we investigated whether the pathogenic mutants AIPL1-A197P and AIPL1-C239R directly interact with FAT10 as well. *In vitro* Co-IP of recombinant proteins revealed that all three recombinant AIPL1 variants were able to directly interact with recombinant FAT10 (Fig. 1B, lanes 3–5). Because FAT10 is a ubiquitin-like modifier containing typical ubiquitin-like folds (28), we tested whether AIPL1 interacts with ubiquitin as well. However, *in vitro* Co-IP studies using recombinant His-tagged ubiquitin and HA-tagged AIPL1, AIPL1-A197P, and AIPL1-C239R showed no interaction of the chaperone with ubiquitin (Fig. S1C), underlining a specific interaction with FAT10.

To confine the interaction sites in more detail, we tested which FAT10 domain is involved in the interaction with AIPL1 (Fig. 1C). HA-GFP–tagged full-length FAT10 (FAT10-GG), the single-FAT10 N-terminal (FAT10-N), or the C-terminal UBD (FAT10-C) were expressed together with FLAG-tagged AIPL1 in HEK293 cells, as indicated. Again, the interaction between AIPL1 and full-length FAT10 was detectable (Fig. 1C, IP:

FLAG, IB: HA, or GFP, lane 6). Interestingly, AIPL1 also interacted with both the N- and the C-terminal FAT10 UBD (Fig. 1C, IP: FLAG, IB: HA, or GFP, lanes 7 and 8), suggesting that both UBDs are used for the interaction. In the negative control, in contrast, no interaction between AIPL1 and GFP was detectable (Fig. 1C, IP: FLAG and IB: GFP, lane 10).

AIPL1 possesses three tetratricopeptide repeat (TPR) motifs that are described to be important for protein-protein interactions (5, 41). To test whether this holds true for FAT10 as well, Co-IP experiments with untagged FAT10 and FLAG-tagged AIPL1 truncation variants were performed (Fig. 1, D and E). Indeed, FAT10 interacted mainly with the TPR motifs, because an interaction was detected only for those AIPL1 truncations still expressing all three TPR motifs. In detail, FAT10 interacted with AIPL1 WT (Fig. 1D, lane 8), AIPL1-S328X (expression of FK506-binding protein (FKBP) and TPR motifs; Fig. 1D, lane 10), AIPL1 TPR (expression of only the TPR motifs; Fig. 1D, lane 11), and slightly with AIPL1 TPR+PRD (expression of the TPR motifs and the C-terminal proline rich domain, Fig. 1D, lane 12). No interaction was observed between FAT10 and the AIPL1-Q163X only expressing the FKBP domain of AIPL1 (Fig. 1D, lane 9). However, the most prominent interaction was detected with AIPL1 WT (Fig. 1D, lane 8), suggesting that proper folding of AIPL1 is important for the interaction with FAT10.

Taken together, our data show that AIPL1 WT interacts not only specifically with FAT10 in a direct manner but also with pathogenic mutants such as AIPL1-A197P and AIPL1-C239R. Moreover, the data demonstrate that AIPL1 interacts via its TPR domains with both FAT10 UBDs (Fig. 1E).
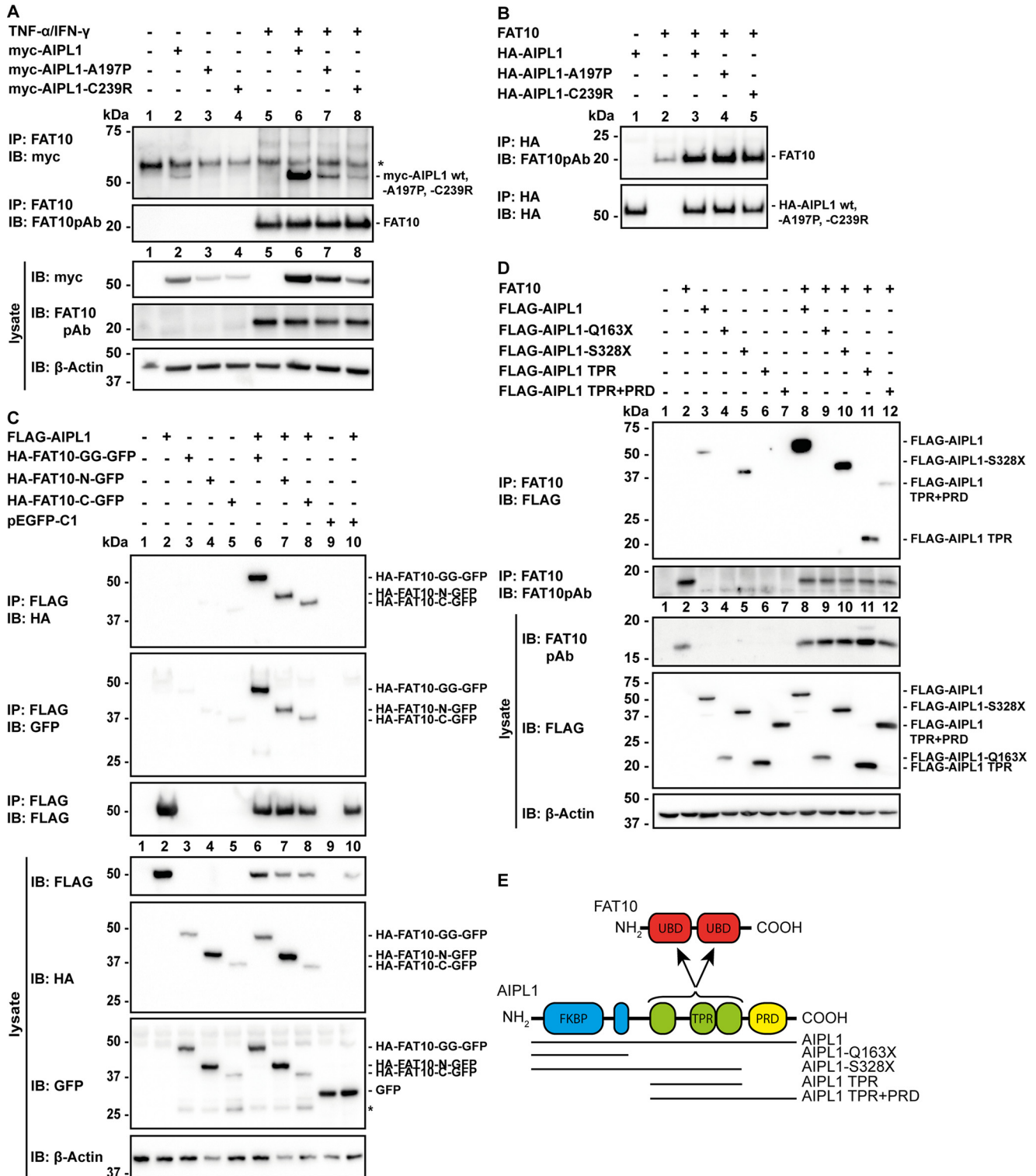
FAT10 mRNA is expressed in human retina

So far, the direct interaction between the ubiquitin-like modifier FAT10 and the retinal chaperone AIPL1 was shown *in vitro* and *in cellulo* (Fig. 1). In general, AIPL1 is expressed only in developing rods and cones, mature rods, and the pineal gland (6–8). Contrary to this, FAT10 mRNA and protein is described to be constitutively expressed in organs of the immune system (25), whereas its expression has not yet been investigated in retinal structures. Because FAT10 expression is inducible in several tissues and cell lines by the pro-inflammatory cytokines TNFα and IFN-γ, we first aimed to test whether FAT10 mRNA expression can also be induced in the retinoblastoma cell line Weri-Rb1 (Fig. 2A). As a control, FAT10 mRNA was markedly increased after stimulating HEK293 cells with TNFα and IFN-γ for 24 h, whereas no mRNA expression was found in untreated cells (Fig. 2A) (34). The same outcome was detected in Weri-Rb1 cells (Fig. 2A). Remarkably, the up-regulation of FAT10 mRNA after induction with TNFα and IFN-γ was even higher than in HEK293 cells.

Showing that FAT10 mRNA expression is inducible in a retinoblastoma cell line led to the suggestion that FAT10 might also be expressed in human retina. To test this, quantitative real-time RT-PCR was performed with three human retina samples. As a control, AIPL1 mRNA expression was prevalent in all three retina samples but not in HEK293 cells (Fig. 2B). Next, FAT10 mRNA expression was measured in noninduced

HEK293 cells, all three donor retinae, and a purchased retinal RNA sample (named hereafter donor 4; Clontech) (Fig. 2*C*). Whereas FAT10 mRNA was not expressed in unstimulated HEK293 cells, it was clearly expressed in three of the four retina samples (Fig. 2*C*, *donors 1*, *2*, *and 4*), indicating that FAT10 mRNA is expressed in human retina. Finally, we also checked mRNA levels of the FAT10-specific E1 activating enzyme

UBA6 and of the E2 conjugating enzyme USE1 (Fig. 2, *D* and *E*). Hereby, mRNA expression in retina samples was again compared with HEK293 cells that are known to express both enzymes (26). We could show that both UBA6 and USE1 were also expressed in human retina although the expression levels fluctuated, probably due to donor variations. Overall, these findings lead to the suggestion that FAT10 is not only expressed
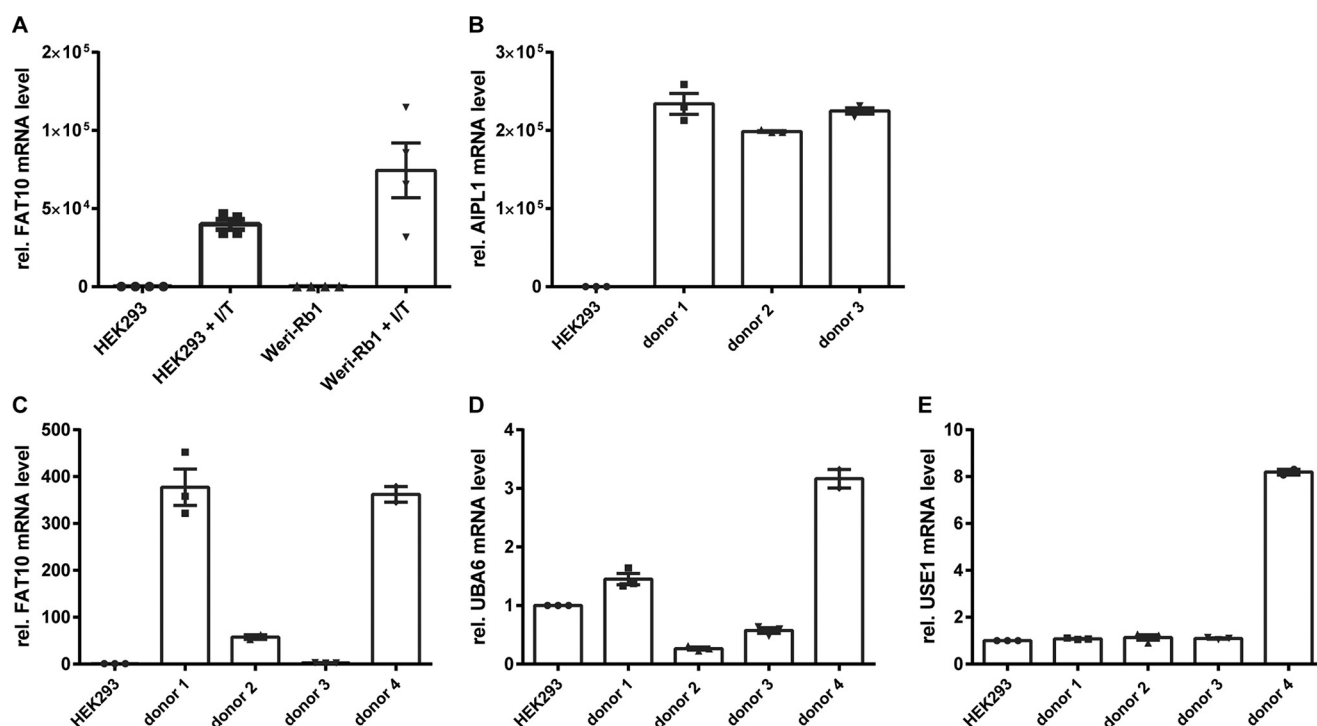
Figure 2. FAT10 mRNA is expressed in human retina. *A*, up-regulation of endogenous FAT10 mRNA in HEK293 and Weri-Rb1 cells upon cytokine treatment with IFN-γ and TNFα (*I/T*) for 24 h. FAT10 mRNA expression was measured by quantitative real-time RT-PCR and normalized to the mRNA expression levels of the housekeeping gene GAPDH. Values of untreated HEK293 cells were set to unity and the other values were calculated accordingly. Data are derived from four independent experiments (*n* = 4); shown is the mean ± S.E (*error bars*). *B–E*, RNA from three retinae (donors 1–3) was extracted and reverse-transcribed into cDNA. Purchased human retina RNA was defined as "donor 4". AIPL1, FAT10, UBA6, and USE1 mRNA expression was measured by quantitative real-time RT-PCR and normalized as described in (*A*). Untreated HEK293 cells served as a control. Triplicates were measured, and shown are the relative mRNA levels as single values and the mean ± S.E (*error bars*).

but might also be activated and conjugated in the human retina.

### The rod phosphodiesterase 6 is a retina-specific FAT10 conjugation substrate

Having shown that FAT10 mRNA is expressed in human retina and that FAT10 protein interacts with the retina-specific chaperone AIPL1, we searched for a retina-specific FAT10 conjugation substrate. Hereby we focused on a known AIPL1 client, the rod PDE6, which is a heterotetramer consisting of one α-subunit (PDE6α), one β-subunit (PDE6β), and two inhibitory γ-subunits (PDE6γ) (3, 10, 12, 16). To investigate rod PDE6 as a possible FAT10ylation target, we amplified the single rod PDE6 subunits out of human retina cDNA and cloned them into expression vectors containing different peptide tags (42). A possible FAT10ylation of the single subunits was tested

by overexpressing the respective subunit together with two different FAT10 variants, His-3xFLAG-FAT10 (further referred to as FLAG-FAT10) and the conjugation-incompetent variant His-3xFLAG-FAT10-AV (FLAG-FAT10-AV) characterized by a C-terminal AV motif replacing the WT GG. The experiments were performed under reducing conditions to visualize both covalent and noncovalent interactions (Fig. 3*B* and Fig. S2) and under denaturing conditions (Fig. 3, *A, C,* and *D*) to further confirm isopeptide formation between FAT10 and the single PDE6 subunits.

After immunoprecipitation of the FAT10 variants, Western blotting analysis showed that His-PDE6α was covalently modified with FAT10 (Fig. 3*A, lane 5*). In contrast, the FAT10-AV mutant was not conjugated to PDE6α (Fig. 3*A, lane 6*). A possible noncovalent interaction with His-PDE6α was detectable for both FAT10 variants (Fig. S2*A, top panel, lanes 5–8*) which was

Figure 1. FAT10 interacts via both UBL domains with the TPR motifs in AIPL1. *A*, HEK293 cells were transiently transfected with expression constructs for myc-AIPL1 variants. FAT10 expression was induced by treating the cells with TNFα (600 units/ml) and IFN-γ (300 units/ml) for 24 h, as indicated. Immunoprecipitation (*IP*) was performed with anti-FAT10 antibody (clone 4F1) coupled to protein A-Sepharose followed by SDS-PAGE and Western blotting analysis (*IB*). *B*, for *in vitro* interaction assays, recombinant FAT10 and HA-tagged AIPL1 variants were incubated in *in vitro* buffer for 60 min at 30 °C, followed by immunoprecipitation using anti-HA agarose. Western blotting analysis was performed using an anti-FAT10 polyclonal antibody. The recombinant protein amounts can be found under "Experimental procedures". *C*, *in cellulo* interaction of FLAG-tagged AIPL1 with different FAT10 truncation versions, namely full-length FAT10 (HA-FAT10-GG-GFP), the N-terminal UBD domain of FAT10 (HA-FAT10-N-GFP), or the C-terminal UBD domain of FAT10 (HA-FAT10-C-GFP). HEK293 cells were transiently transfected with expression constructs for the indicated proteins. Immunoprecipitation using anti-FLAG M2 affinity gel was followed by Western blotting analysis. *D*, to identify the FAT10 binding site in AIPL1, co-immunoprecipitations of FLAG-AIPL1 truncation variants and FAT10 were performed in transiently transfected HEK293 cells. Anti-FAT10 antibody (clone 4F1) coupled to protein A-Sepharose was used for immunoprecipitation. *E*, schematic illustration of the interaction of FAT10 and AIPL1. Shown are both UBD domains of FAT10 (*red*), AIPL1 FKBP (*blue*), TPR (*green*), the proline-rich (*yellow*) domain, and the tested pathogenic AIPL1 mutants. For all experiments, *asterisks* mark unspecific background binding, and one representative experiment of three experiments with similar outcomes is shown.
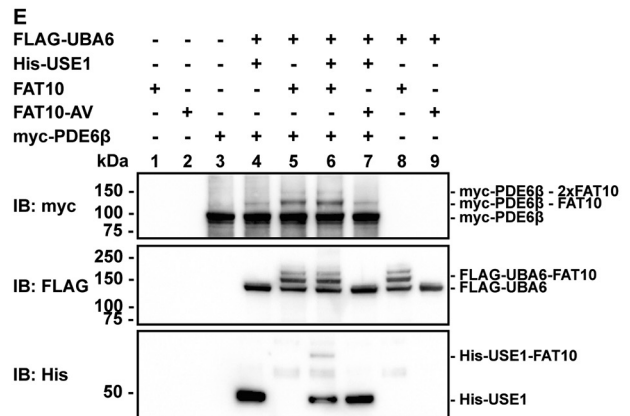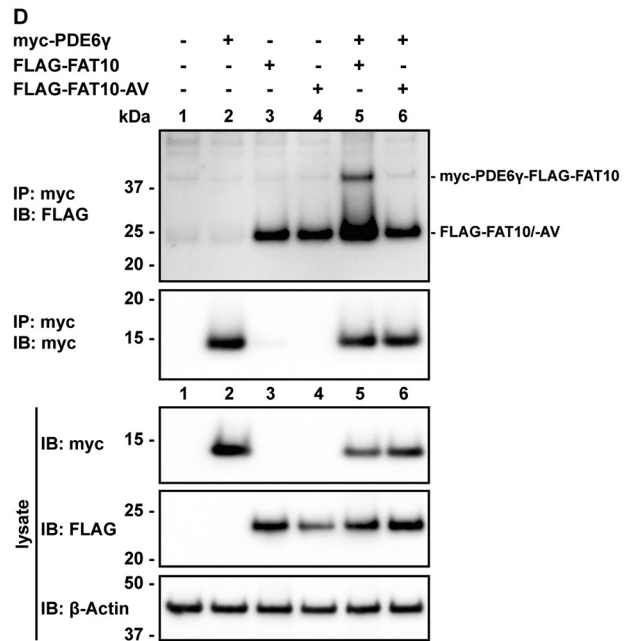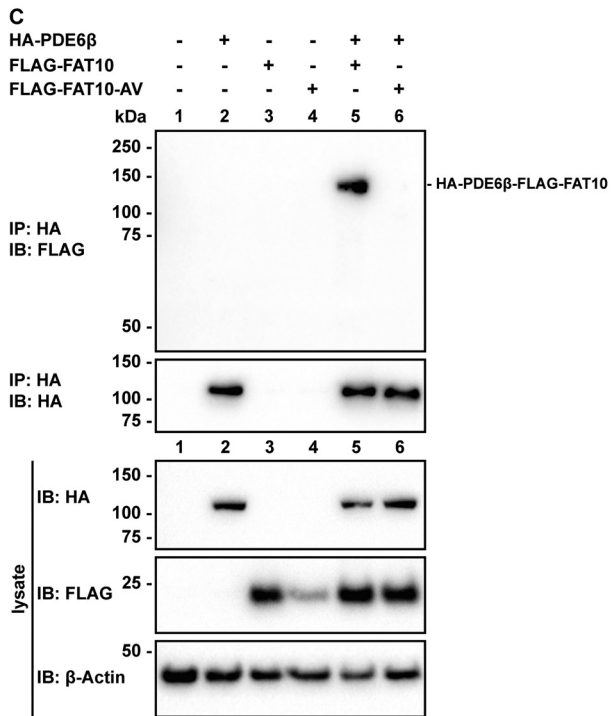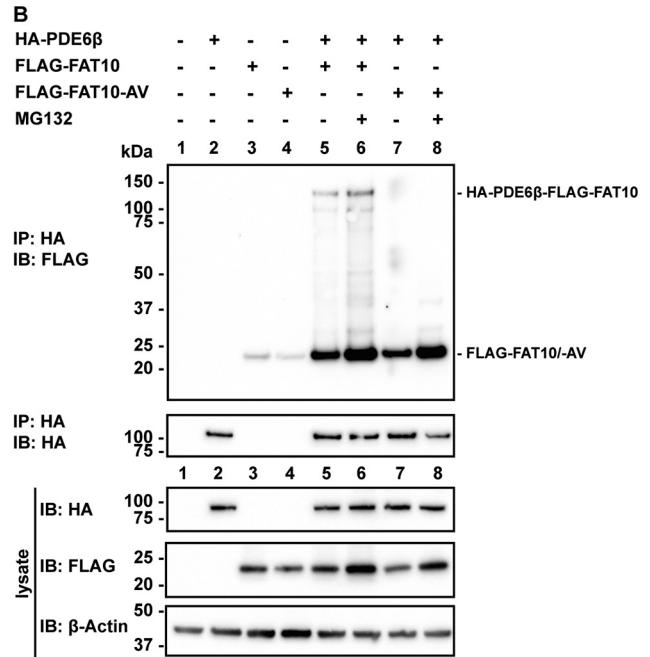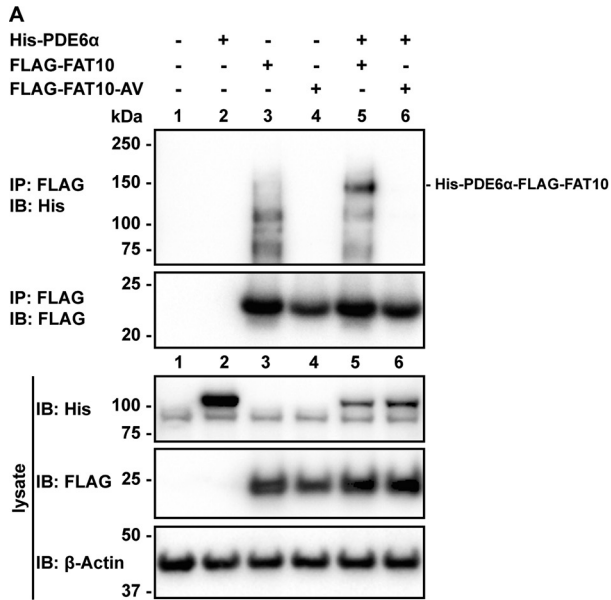
independent of the C-terminal diglycine motif of FAT10. Of note, during inhibition of the proteasome with MG132, the amount of PDE6α-FAT10 conjugate increased (Fig. S2A, *lane 6*), indicating that FAT10ylation of PDE6α might lead to its proteasomal degradation.

Accordingly, the other catalytic subunit PDE6β was tested as a possible FAT10 conjugation substrate. An isopeptide-linked PDE6β-FAT10 conjugate was detected under reducing (Fig. 3B, *lanes 5 and 6*) and under denaturing conditions (Fig. 3C, *lane 5*). Additionally, a noncovalent interaction occurred between both FAT10 variants and PDE6β (Fig. 3B, *top panel, lanes 5–8*). FAT10ylation of PDE6β was likewise dependent on the C-terminal diglycine motif because it was not detectable with the FAT10-AV mutant (Fig. 3B, *lanes 7 and 8* and Fig. 3C, *lane 6*). Inhibition of the 26S proteasome led to only a slight increase in the PDE6β-FAT10 conjugate amount (Fig. 3B, *lane 6*), consistent with a proteasomal degradation of the conjugate. Performing the same experiment using a low-percentage SDS-PAGE revealed that PDE6β not only became FAT10ylated with one FAT10 moiety but seemed to be oligo mono-FAT10ylated with at least two FAT10 molecules (Fig. S2B, *lanes 5–8*). Because no difference was observed between FAT10 WT and a FAT10 variant lacking all internal lysine residues, FAT10 K0, it can be presumed that several single-FAT10 proteins were covalently conjugated to the subunit and that no FAT10 chain was built (Fig. S2B, *lanes 5 and 6 versus lanes 7 and 8*). As already seen in previous experiments, proteasomal inhibition with MG132 led to an accumulation of the conjugate (Fig. S2B, *top panel*).

Completing this study for all PDE6 components, we investigated a possible FAT10ylation of the inhibitory PDE6γ subunit (Fig. 3D). In line with the catalytic subunits PDEα and PDE6β, a covalent FAT10ylation of PDE6γ was detectable under denaturing (Fig. 3D, *lane 5*) and under reducing conditions (Fig. S2C, *lanes 5 and 6*). This was likewise dependent on the C-terminal diglycine motif (Fig. 3D, *lane 6* and Fig. S2C, *lanes 7 and 8*). No clear statement can be drawn concerning a possible non-covalent interaction between PDE6γ and FAT10, because His-3xFLAG-tagged FAT10 showed a high unspecific background binding to the myc-beads (Fig. 3D and Fig. S2C).

To investigate whether PDE6β becomes FAT10ylated not only *in cellulo* but also under *in vitro* conditions, recombinant FLAG-UBA6, His-USE1, FAT10, FAT10-AV, and myc-PDE6β were incubated at 30 °C followed by Western blotting analysis (Fig. 3E). With this approach, a PDE6β-FAT10 conjugate was detected in the presence of UBA6 and USE1 (Fig. 3E, *lane 6*), showing that PDE6β is also covalently modified with FAT10 *in vitro*. No FAT10ylation of PDE6β was observable with the FAT10-AV mutant (Fig. 3E, *lane 7*). Moreover, an oligo

mono-FAT10ylation of the recombinant myc-PDE6β with two FAT10 moieties could be detected, which is in line with the *in cellulo* data (Fig. S2B). Interestingly, PDE6β was also FAT10ylated in the absence of the E2 conjugating enzyme USE1 (Fig. 3E, *lane 5*), indicating that at least *in vitro* UBA6 alone was sufficient to mediate the FAT10 transfer onto PDE6β as recently published by our group for other substrates (39, 40).

Taken together, our data identify rod PDE6 as a retina-specific FAT10 conjugation substrate. Both rod PDE6 catalytic subunits, PDE6α and PDE6β, as well as the inhibitory PDE6γ subunit become covalently modified with FAT10. Additionally, PDE6α and PDE6β also interact noncovalently with FAT10.

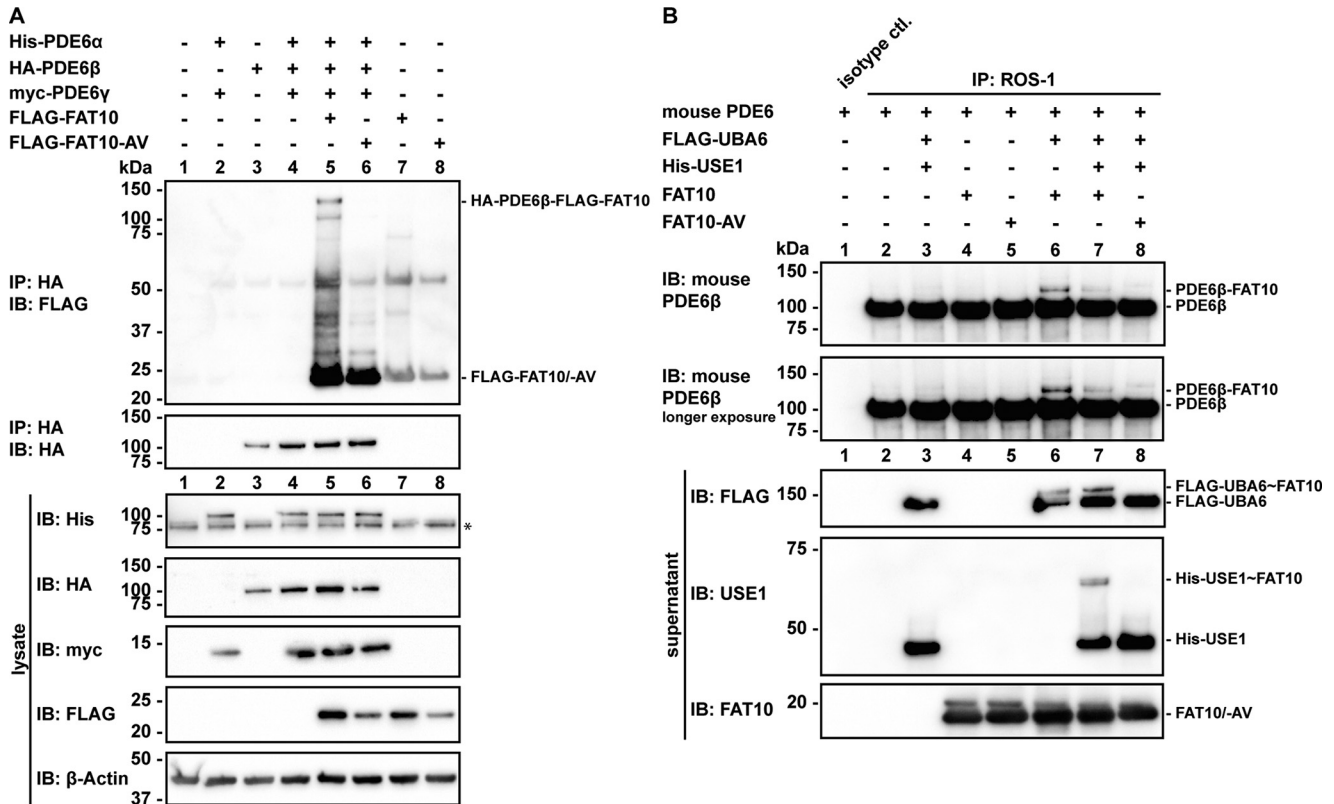### The PDE6β subunit is also FAT10ylated when incorporated in the holoenzyme

So far, only FAT10ylation of single PDE6 subunits had been investigated, raising the question whether a properly formed PDE6 holoenzyme might be modified with FAT10 as well. Therefore, we overexpressed all three rod PDE6 subunits together with either FAT10 WT or the FAT10-AV mutant in HEK293 cells. In accordance with our previous publication where co-localization of the ectopically expressed PDE6 subunits had been shown by confocal microscopy (42), the interaction of the single subunits was confirmed by Co-IP experiments, pointing to a formation of the PDE6 holoenzyme upon ectopic expression of the subunits in HEK293 cells (Fig. S3, *A and B*).

Combined immunoprecipitation and Western blotting analysis under reducing conditions (4% β-mercaptoethanol (2-ME)) revealed that PDE6β, although it interacted with the other subunits and was eventually incorporated in the holoenzyme, was indeed FAT10ylated (Fig. 4A, *lane 5*). As already seen before, no signal was obtained with the FAT10-AV mutant (Fig. 4A, *lane 6*). However, both FAT10 variants were still able to noncovalently interact with PDEβ (Fig. 4A, *lanes 5 and 6*). This led to the suggestion that incorporation of the β-subunit into a holoenzyme complex or interaction of PDE6β with other subunits does not prevent its covalent modification with FAT10.

Nonetheless, it cannot be excluded that only free PDE6β was FAT10ylated in our experimental setup. Unfortunately, no antibody for the immunoprecipitation of human PDE6 holoenzyme is available and recombinant purification of the fully assembled human enzyme has not been established so far. We circumvented these issues by using mouse PDE6 enzyme because mouse and human PDE6β share 93% sequence similarity at the amino acid level. C57BL/6 mouse retina was prepared and lysed, and PDE6 was immunoprecipitated with the ROS-1

Figure 3. The rod PDE6 is a retina-specific FAT10 conjugation substrate. *A, C,* and *D,* HEK293 cells were transiently transfected with expression constructs for His-3xFLAG-FAT10 (*FLAG-FAT10*), His-3xFLAG-FAT10-AV (*FLAG-FAT10-AV*), and the indicated PDE6 subunit. The experiment was performed under denaturing conditions with 2% SDS and 10 mM NEM in the lysis buffer. Immunoprecipitations were performed using anti-FLAG M2 affinity gel, anti-HA agarose, or anti-c-myc affinity gel. SDS-PAGE under reducing conditions with 4–12% gradient gels (NuPAGE) was followed by Western blotting analysis using the respective antibodies. β-actin served as a loading control. Shown are single experiments of three experiments each with similar outcomes. *B,* the experiment was performed as described in (*C*), but under reducing conditions (4% 2-ME in the gel sample buffer). *E, in vitro* FAT10ylation of PDE6β. Recombinant proteins were incubated for 60 min at 30 °C in an ATP-containing *in vitro* buffer. The reaction was stopped with 5× SDS gel sample buffer containing 4% 2-ME, followed by SDS-PAGE and Western blotting analysis. The recombinant protein amounts can be found under "Experimental procedures". Shown is one experiment of two (*A* and *D*) or three (*B, C, E*) experiments with similar outcomes.

Figure 4. The PDE6β subunit is also FAT10ylated when incorporated in the holoenzyme. *A,* PDE6 FAT10ylation under overexpression conditions in HEK293 cells. The cells were transiently transfected with expression constructs for all rod PDE6 subunits, FLAG-FAT10, or FLAG-FAT10-AV. An immunoprecipitation against HA-PDE6β was performed and the samples were separated on 4–12% gradient gels (NuPAGE) followed by Western blotting analysis. Unspecific background is marked with an *asterisk*. *B,* conjugation of FAT10 to mouse PDE6 holoenzyme. Retinae from C57BL/6 mice were prepared and lysed in RIPA buffer. Mouse PDE6 holoenzyme was immunoprecipitated overnight with ROS-1 antibody coupled to protein A-Sepharose. Mouse IgG2a was used as an isotype control for the immunoprecipitation. Immunoprecipitated PDE6 was used in an *in vitro* FAT10ylation assay with recombinant proteins, as indicated. Reactions were incubated at 30 °C for 30 min. Supernatant samples were analyzed under nonreducing conditions, and immunoprecipitation samples were analyzed under reducing conditions using 4–12% gradient gels (NuPAGE) and the respective antibodies. The recombinant protein amounts can be found under "Experimental procedures." Shown is one experiment of three experiments with similar outcomes, respectively.

antibody that is described to only recognize fully assembled mouse PDE6 (43). The immunoprecipitated PDE6 was further used for *in vitro* FAT10ylation assays using recombinant human FAT10, UBA6, and USE1 (50% input of the recombinant proteins used is shown in Fig. S3C). Thereby we could show that PDE6β was clearly FAT10ylated with FAT10 WT but not with FAT10-AV (Fig. 4B, *lanes 6–8*). As already shown above, UBA6 alone was sufficient for PDE6β FAT10ylation (Fig. 4B, *lane 6*). Similar amounts of FAT10 and FAT10-AV were used, whereas only FAT10 was activated by UBA6 and transferred onto USE1 (Fig. 4B, *supernatant*).

These data confirm that the catalytic β-subunit of PDE6 becomes FAT10ylated despite its incorporation into the holoenzyme.

AIPL1 stabilizes FAT10 and the PDE6β-FAT10 conjugate

Because PDE6 is a client of the chaperone AIPL1, we investigated whether AIPL1 has an impact on the FAT10ylation of this enzyme. During their studies, Bett *et al.* (21) reported that FAT10 accumulates in the presence of AIPL1. Therefore, we performed a cycloheximide (CHX) chase experiment to monitor the stability of monomeric FAT10 protein in the absence or presence of AIPL1 WT or AIPL1-A197P (Fig. 5A). Treatment of cells with

CHX for the indicated time periods inhibited protein *de novo* synthesis giving the possibility to track the degradation of proteins. In line with the reported observation, a slower degradation rate for monomeric FAT10 was observed when AIPL1 WT was co-expressed (Fig. 5A, *lanes 4–6 versus lanes 1–3*). Interestingly, the pathogenic mutant AIPL1-A197P likewise stabilized FAT10 (Fig. 5A, *lanes 7–9 versus lanes 1–3*), indicating that the direct interaction with FAT10 (Fig. 1) is sufficient for its stabilization.

In the next step, the formation of the PDE6β-FAT10 conjugate was investigated in the presence of different AIPL1 variants (Fig. 5B). Again, an accumulation of FAT10 in the presence of all AIPL1 variants was detectable (Fig. 5B, *lysate IB: FLAG, lanes 8–10*). Interestingly, the amount of PDE6β also increased in the presence of all AIPL1 variants (Fig. 5B, *lysate IB: HA, lanes 8–10*). In line with this, more PDE6β-FAT10 conjugate, and especially an increased noncovalent interaction between FAT10 and PDE6β, was observed in the presence of AIPL1, AIPL1-A197P, and AIPL1-C239R (Fig. 5B, *top panel, lanes 7–10*). This led to the suggestion that AIPL1, FAT10, and PDE6β might build a trimeric complex based on the interaction between FAT10 and AIPL1, resulting in a stabilization of the modifier and, in consequence, of the FAT10 conjugation substrate.

In addition, we could show that the stabilization of the conjugate depended on the amount of AIPL1 (Fig. 5C). Upon
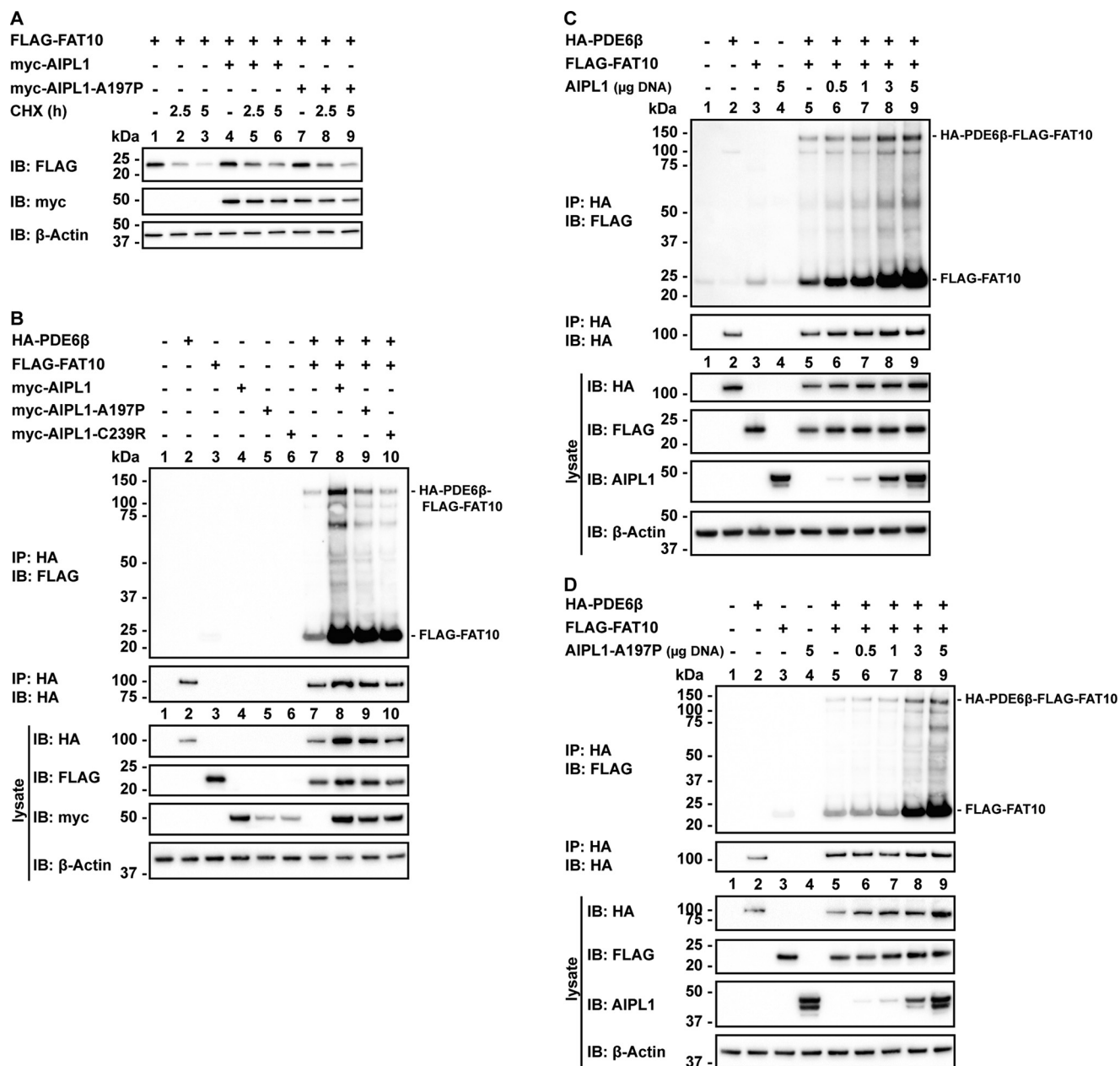
Figure 5. AIPL1 stabilizes FAT10 and the PDE6β-FAT10 conjugate. *A,* Western blotting analysis showing the degradation rate of monomeric FAT10 analyzed in HEK293 cells co-expressing myc-tagged AIPL1 or AIPL1-A197P. Before harvesting, cells were treated for 2.5 or 5 h with 50 μg/ml CHX to inhibit protein *de novo* synthesis. One experiment of three experiments with similar outcomes is shown. *B,* HEK293 cells were transiently transfected with expression constructs for HA-PDE6β, FLAG-FAT10, myc-AIPL1, myc-AIPL1-A197P, and myc-AIPL1-C239R, as indicated. After cell lysis, HA-PDE6β was immunoprecipitated with anti-HA agarose and proteins were separated under reducing conditions using 4–12% gradient gels (NuPAGE). FAT10ylation of PDE6β was visualized by Western blotting analysis. Shown is one experiment of three experiments with similar outcomes. *C* and *D,* investigation of PDE6β FAT10ylation was performed as described in (*B*) but with increasing amounts of expression constructs (0.5– μg of DNA) for untagged AIPL1 WT (*C*) or AIPL1-A197P (*D*). One experiment of three (AIPL1 WT; *C*) or of two (AIPL1-A197P; *D*) experiments with similar outcomes is shown.

transfection of cells with fixed plasmid amounts for HA-PDE6β and FLAG-FAT10 but increasing amounts of plasmid DNA encoding for AIPL1, more covalent and noncovalent interaction between PDE6β and FAT10 was detectable, correlating with the increasing amounts of AIPL1 (Fig. 5C, *top panel*). Consistent with that, amounts of FAT10 and PDE6β were elevated upon stronger expression of AIPL1 (Fig. 5C, *lysate IB: HA and IB: FLAG, lane 9 versus lane 5*). The same results were obtained when expressing the AIPL1 mutant AIPL1-A197P (Fig. 5D).

In summary, we showed that the degradation rate of monomeric FAT10 was slowed down in the presence of AIPL1 WT or AIPL1-A197P, resulting in an increased PDE6β-FAT10 conjugate formation that depended on the concentration of AIPL1.

FAT10 targets PDE6 for proteasomal degradation

FAT10ylation of substrates targets them for degradation by the 26S proteasome (36, 38). We wanted to know whether this holds true for PDE6β because we saw a slight increase in
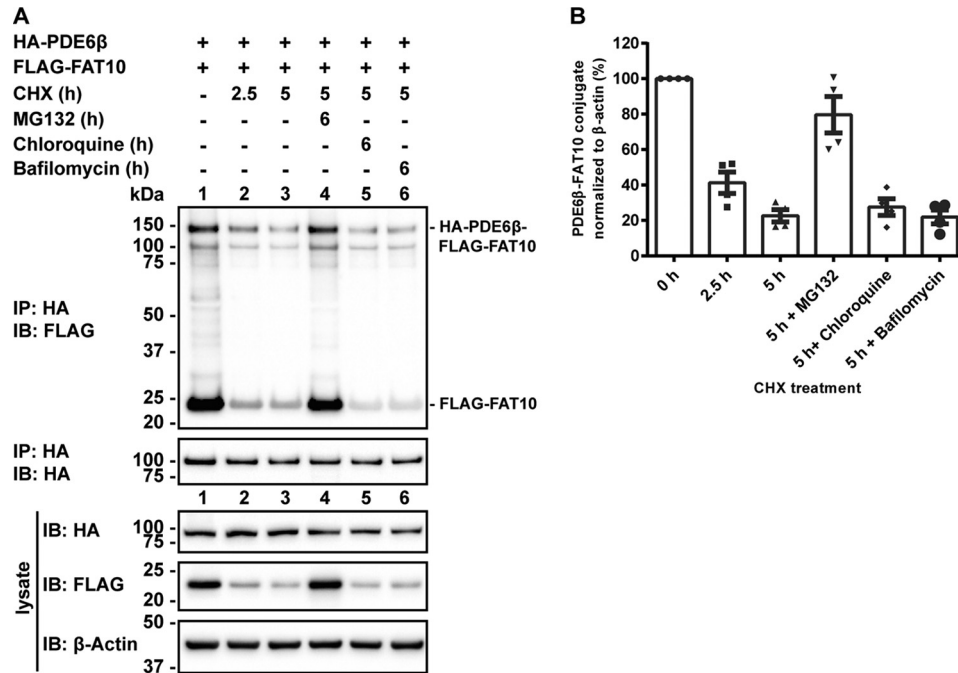
Figure 6. FAT10 targets PDE6 for proteasomal degradation. *A*, the degradation rate of PDE6β-FAT10 conjugate in transiently transfected HEK293 cells 24 h after transfection was monitored by treating the cells with CHX (50 μg/ml; 2.5 or 5 h). When indicated, the cells were additionally treated for 6 h prior to harvesting with MG132 (10 μM) to block proteasomal degradation or with bafilomycin A1 (0.2 μM) or chloroquine (100 μM) to interfere with lysosomal degradation. Immunoprecipitation was performed using anti-HA agarose, and proteins were separated under reducing conditions. One representative experiment of four experiments with similar outcomes is shown. *B*, densitometric analysis of ECL signals of CHX chase experiments. ECL signals of PDE6β-FAT10 conjugate were normalized to the ECL signals of β-actin. The values of untreated cells were set to unity. Shown is the mean $\pm$ S.E. (*error bars*) of four experiments with similar outcomes ($n = 4$).

PDE6β-FAT10 conjugate upon proteasomal inhibition (Fig. 3B). To verify proteasomal degradation of the PDE6β-FAT10 conjugate, we performed CHX chase experiments with HEK293 cells transiently expressing HA-PDE6β and FLAG-FAT10 (Fig. 6A). As a control, MG132 was added to block the catalytic activity of the 26S proteasome (Fig. 6A, *lane 4*). Moreover, endosomal acidification and maturation of autophagic vacuoles were inhibited with chloroquine or bafilomycin A1, respectively (Fig. 6A, *lanes 5 and 6*). In line with previous data ((26) and Fig. 5A), monomeric FAT10 was almost completely degraded within 5 h of chase whereas its degradation was rescued upon proteasome inhibition (Fig. 6A, *lysate IB: FLAG, lane 3 versus lane 4*). Likewise, the PDE6β-FAT10 conjugate was degraded over time and rescued by proteasomal inhibition, although the amount of rescued protein was not quite as high as for monomeric FAT10 (Fig. 6A, *top panel*). Because monomeric FAT10 itself is degraded over time, only small amounts could be additionally conjugated to PDE6β during the time of CHX treatment. Considering that no FAT10-specific deconjugating enzyme has been found and that covalent conjugation of FAT10 targets the bulk of its substrates to proteasomal degradation at the same pace as monomeric FAT10 (36, 38), the observed decline of PDE6β-FAT10 conjugate over time is very likely due to proteasomal degradation. As treatment of cells with neither chloroquine nor bafilomycin A1 affected the degradation, an involvement of lysosomal degradation or autophagy could be excluded (Fig. 6A, *top panel, lanes 5 and 6* and densitometric analysis in Fig. 6B). Densitometric analysis of the ECL signals of the conjugate normalized to the levels of β-actin

in the respective lanes revealed that ~50% of the conjugate was degraded after 2.5 h of CHX treatment (Fig. 6B).

Altogether, FAT10ylation of PDE6β targets PDE6β for proteasomal degradation as already documented for other FAT10 substrates (35).

Noncovalent interacting FAT10 inhibits PDE6 activity

To gain insight into whether FAT10 has an impact on the functionality of PDE6 in addition to targeting it for proteasomal degradation, we first examined the FAT10ylation site within PDE6β. To this aim we co-expressed FLAG-FAT10 together with truncated PDE6β mutants (Fig. 7, *A and B*). The N-terminal GAFa domain alone (HA-PDE6β GAFa), both GAF domains (HA-PDE6β GAFa+b), or only the C-terminal catalytic PDEase domain (HA-PDE6β PDEase) were expressed. Full-length PDE6β was used as a control. Co-IP of the HA-tagged PDE6β truncations and subsequent Western blotting analysis showed that FAT10 interacted with all expressed domains in a noncovalent manner (Fig. 7B, *lane 7–10*). As expected, full-length PDE6β was strongly FAT10ylated (Fig. 7B, *lane 10*). In addition, a covalent modification was observed for the GAFa domain and for the PDEase domain (Fig. 7B, *lanes 7 and 9*). In the case of GAFa+b, a single band was detected at around 75 kDa, most likely representing mono-FAT10ylation in the GAFa domain because it could be shown that this domain is even FAT10ylated when expressed solely (Fig. 7B, *top panel, lane 7*). Unspecific binding to HA agarose, as frequently observed for FAT10, explains the background signal in *lane 2* (Fig. 7B, *top panel, lane 2*). As a control, repetition of the

Figure 7. Noncovalent interacting FAT10 inhibits PDE6 activity. *A*, schematic illustration of PDE6β domains and truncation forms analyzed. *B*, HEK293 cells transiently expressing FLAG-FAT10 and different HA-tagged PDE6β truncations. Cleared lysates were subjected to immunoprecipitation of HA-PDE6β truncations. FAT10ylation of PDE6β variants was visualized by Western blotting after separating the proteins under reducing conditions on 4–12% gradient gels. Shown is one of three experiments with similar outcomes. *C*, cGMP hydrolysis assay in the presence or absence of FAT10 using mouse PDE6. Retina from five C57BL/6 mice were prepared, lysed in phosphate-free lysis buffer, and desalted using PD Mini Trap G-25 columns. Production of 5′-GMP was measured by subsequent enzymatic cleavage of 5′-GMP into the nucleoside and phosphate via a 5′-nucleotidase. The amount of released phosphate was quantified with a colorimetric reaction in a modified Malachite Green assay by measuring the absorbance at 620 nm. As inhibitors, recombinant FAT10 ((+) = 1.67 µg, (++) = 5 µg) or FAT10-AV ((++) = 1.5 µg, (++) = 4.5 µg) were added. FAT10 storage buffer served as a control. Shown is the mean ± S.E. (*error bars*) of five experiments (*n* = 5). Significance was calculated using one-way analysis of variance with Dunnett correction. A *p* value of ****$p < 0.0001$ was considered to be highly statistically significant. *D*, absorbance was measured during the 30 min of colorimetric reaction for the experiment described in (*C*). Shown is the mean ± S.E. (*error bars*) of five experiments (*n* = 5).

experiment using FAT10-AV instead of FAT10 WT showed no covalent isopeptide linkages between FAT10 and different PDE6β versions, whereas noncovalent interactions were not affected (Fig. S4*A*). This is in line with our finding of oligo mono-FAT10ylation of the PDE6β subunit (Fig. S2).

Within the PDE6β subunit, the GAFa domain is important for cGMP binding, whereas the PDEase domain possesses the catalytic activity for hydrolysis of cGMP. Moreover, the inhibitory PDE6γ subunits bind to these two domains (14, 44). Because we saw that FAT10 is able to interact with these two important domains in a covalent but also a noncovalent manner, we investigated a possible influence of FAT10 on the activity of PDE6 using a cGMP hydrolysis assay. Briefly, PDE6 activity was measured by using a defined amount of cGMP as a substrate. After hydrolysis of cGMP by PDE6, a supplemented 5′-nucleotidase enzymatically cleaves 5′-GMP into the nucleoside and phosphate, which in turn can be detected in a colorimetric assay by measuring the absorbance at 620 nm. To ensure a high amount of functional enzyme in the assay, lysate of

mouse retina served as a source for PDE6 holoenzyme whereas recombinant human FAT10 was used to test a possible influence of the modifier onto the PDE6 activity. Retinae of five C57BL/6 mice were prepared and lysed in a phosphate-free lysis buffer, and protein amounts were comparable for all prepared retinae as seen in a colloidal Coomassie staining of whole retina lysate (Fig. S4*B*). A control Western blotting analysis using the mouse retinal lysates showed similar PDE6β expression levels (Fig. S4*C*), indicating that comparable amounts of PDE6 were used in the assay.

After the reaction and incubation with the reagent reacting with free phosphate for 30 min, the absorbance at 620 nm was measured and amounts of produced 5′-GMP were calculated (Fig. 7*C*). Recombinant enzyme of PDE class I served as a positive control and revealed that the enzyme was active and able to hydrolyze cGMP (Fig. 7*C*, *PDE*), confirming the functional experimental setup. To ensure that impurities in neither the FAT10 or FAT10-AV preparations nor the FAT10 storage buffer itself influenced the system, cGMP was incubated only

with recombinant FAT10, FAT10-AV, or buffer. Because no enhanced amounts of 5′-GMP could be detected, it can be concluded that the proteins themselves did not influence cGMP turnover (Fig. 7C, *FAT10*, *FAT10-AV*, and *FAT10 buffer*). In addition, the background signal within the lysates was measured and revealed that the phosphate-free lysis and subsequent desalting was successful because no background was detectable (Fig. 7C, *lysate w/o substrate*). Incubation of mouse retina lysate with cGMP resulted in an increased absorbance and accordingly increased amounts of 5′-GMP, indicating that mouse PDE6 successfully hydrolyzed its substrate (Fig. 7C, *lysate*). Strikingly, the addition of increasing amounts of FAT10 significantly decreased cGMP turnover in a dose-dependent manner (Fig. 7C, *lysate + FAT10 (+)* and *lysate + FAT10 (++)*). Thus, FAT10 has a suppressive impact on PDE6 activity. To check whether the inhibition depends on the covalent FAT10ylation of PDE6, we used comparable amounts of the conjugation defective mutant FAT10-AV. Interestingly, FAT10-AV was as potent as FAT10 WT and significantly reduced PDE6 activity (Fig. 7C, *lysate + FAT10-AV (+)* and *lysate + FAT10-AV (++)*). This showed that the noncovalent interaction between FAT10 and PDE6 was sufficient for PDE6 impairment. When measuring the absorbance starting from the beginning of the colorimetric reaction over a time period of 30 min, the same result was obtained (Fig. 7D). Whereas a strong PDE6 activity was measurable in the absence of FAT10 variants or in the presence of FAT10 buffer, a strong decrease was observed with FAT10 or FAT10-AV (Fig. 7D, *lysate + FAT10/FAT10-AV (+)*). This decrease was even more prominent with higher amounts of FAT10 (Fig. 7D, *FAT10/FAT10-AV (++)*).

Taking all results together, we have shown that FAT10 mRNA is expressed in human retina and we suggest that its expression is inducible in retina under inflammatory conditions. Up-regulation of FAT10 enables the covalent modification of the enzyme PDE6 whereby PDE6-FAT10 conjugates are stabilized by AIPL1. FAT10 protein expression has two different functional consequences for PDE6. Whereas covalent modification targets PDE6 to proteasomal degradation, the noncovalent interaction of FAT10 with PDE6 down-regulates PDE6 function, thus resulting in a reduction of cGMP hydrolysis.

Discussion

The retinal chaperone AIPL1 is very important for the maintenance of retinal phototransduction in photoreceptors, and a loss of AIPL1 leads to rapid degeneration of rods and cones (45). Single point mutations in the *Aipl1* gene cause the retinal dystrophy LCA, resulting in the degeneration of photoreceptors (6). Recently, a connection between AIPL1 and the ubiquitin-like modifier FAT10 was identified (21). Considering that AIPL1 is only expressed in photoreceptor cells and the pineal gland (6–8), we investigated a possible role of FAT10 in photoreceptor cells. Our data revealed that FAT10 mRNA is indeed expressed in the retina and that the rod PDE6 protein is a target of FAT10ylation and a noncovalent interaction partner of the FAT10 protein, leading either to proteasomal degradation of PDE6 or to a decreased PDE6 cGMP hydrolysis activity.

In our previous publication we had shown that AIPL1 interacts with FAT10 in a noncovalent manner (21). We now confirmed these findings and characterized this interaction further, showing that AIPL1 binds to both UBL domains of FAT10 (Fig. 1C). This is in contrast to other FAT10 interaction partners such as negative regulator of ubiquitin-like proteins 1 (NUB1), which was shown to bind only to the N-terminal UBL domain of FAT10 (46). In line with other AIPL1 interaction partners, FAT10 was also interacting with the AIPL1 TPR motifs that are already described to be important for protein-protein interactions (Fig. 1D) (41, 47). Interestingly, neither point mutations within the TPR domain (A197P and C239R) nor mutations in any other domain of AIPL1 (*e.g.* R38C in FKBP and P376S in the proline-rich domain) influenced the interaction with FAT10 (Fig. 1 and Fig. S1, *A and B*). Because AIPL1 binds both FAT10 UBD domains (Fig. 1C), it seems likely that FAT10 binds to multiple sites within the TPR region, diminishing the effect of a single point mutation. Interestingly, no interaction of AIPL1 with ubiquitin was observed *in vitro* (Fig. S1C). This might be explained by the fact that the surface charge distributions of ubiquitin and FAT10 differ entirely from each other (28). Hereby, the hydrophobic patch in ubiquitin (Leu-8, Ile-44, and Val-70) that serves in most cases for ubiquitin-protein interactions is conserved in neither the FAT10-N nor the FAT10-C domain. Because we could show that AIPL1 is able to interact with both the N- and C-terminal UBDs of FAT10, one could further speculate that the single UBD of ubiquitin is not sufficient for a stable interaction with AIPL1.

So far, FAT10 expression in retinal cells has not been investigated. Here we provide data that FAT10 mRNA expression is inducible in the retinoblastoma cell line Weri-Rb1 upon cytokine treatment with TNFα and IFN-γ (Fig. 2A). We further show FAT10 mRNA expression in human retina samples (Fig. 2C). Here, one has to keep in mind that the retina is a multilayer structure including different cell types. However, the precise cell type expressing FAT10 could not be determined because of the lack of a suitable antibody reactive against mouse FAT10 that would be sensitive and specific enough to visualize endogenous mouse FAT10 in immunostainings of mouse retina. Likewise, difficulties in obtaining human retina samples hindered us from performing additional biochemical interaction studies for human AIPL1 and FAT10. However, because FAT10 mRNA expression was not detectable in every donor sample and because it can be excluded that donors of the retinal tissues suffered from a known retinopathy, it can be suggested that FAT10 might not be constitutively expressed but rather is up-regulated as a consequence of inflammation. Therefore, it cannot be excluded that FAT10 mRNA and protein expression is also induced during the pathogenesis of retinopathies such as LCA. Increased levels of cGMP caused by the inhibition of PDE6 with the drug Zaprinast in porcine retinal explants resulted in the production of TNFα and IL-6 (48), a cytokine combination that was shown to induce FAT10 expression in HepG2 cells (49). This leads to the hypothesis that FAT10 might be expressed in the retina of LCA patients due to unproductive PDE6 assembly caused by pathogenic AIPL1 mutants which in turn cause an inflammatory environment enabling FAT10 induction that further aggravates the situation.

We have identified the rod PDE6 as the first retina-specific FAT10 conjugation substrate (Fig. 3) targeting PDE6 to proteasomal degradation (Fig. 6) as already seen for other FAT10 substrates such as the ubiquitin E1 activating enzyme UBE1, the transcription factor JunB, or the ubiquitin deconjugating enzyme OTUB1 (35, 39, 40). Because AIPL1 is a chaperone for PDE6 (3), we investigated whether AIPL1 might influence PDE6 FAT10ylation. Indeed, we showed that both AIPL1 WT and AIPL1-A197P stabilized monomeric FAT10 and thus also the PDE6β-FAT10 conjugate (Fig. 5). In contrast, no significant differences between AIPL1 WT and pathogenic AIPL1 mutants causing LCA were observed concerning their interaction with FAT10 or their ability to stabilize FAT10ylated PDE6. It should be kept in mind, however, that FAT10 interacts strongly with negative regulator of ubiquitin-like proteins 1 (NUB1), which is highly expressed in the brain and accelerates the degradation of FAT10 and FAT10 conjugates by the 26S proteasome (46, 50). Because NUB1 was shown to bind to WT AIPL1 but not to LCA causing variants of AIPL1 (47), it is quite possible that binding of NUB1 to AIPL1 is required to more effectively sequester FAT10 and keep it from inhibiting PDE6 or from mediating its degradation. This possibility is currently experimentally addressed in our laboratory. Importantly, AIPL1 and PDE6 are exclusively expressed in rod and cone photoreceptors within the retina (3, 7, 8). Therefore, the identification of AIPL1 as an interaction partner and PDE6 as a substrate of FAT10 conjugation led to the suggestion that FAT10 itself is expressed by the photoreceptors functioning in the maintenance of proteostasis during phototransduction.

So far, it is not clear where FAT10 is localized within photoreceptors. Because AIPL1 is expressed in the inner segment and is not readily detected in the outer segment (7), one possibility would be that it captures FAT10 and hinders its movement to the outer segment. Within this study, an inhibitory effect of FAT10 onto the PDE6 activity was found (Fig. 7). Although whole retina lysate was used for the investigation, one can assume that FAT10 specifically inhibited PDE6 activity, because to our knowledge PDE6 is the only cGMP-specific class of PDE expressed in photoreceptors of the retina (51). Showing that FAT10 influences PDE6 activity by its noncovalent interaction resulting in a decreased cGMP hydrolysis (Fig. 7), hindrance of FAT10 translocation into the outer segment would help to maintain PDE6 function within the already exported PDE6 in the disc membranes. Additionally, we saw an accumulation of PDE6β-FAT10 conjugate in the presence of AIPL1, suggesting that a trimeric complex of PDE6, FAT10, and AIPL1 is formed. Thereby FAT10ylated PDE6 might be retained in the inner segment. Thus, eventually, reduced amounts of PDE6 in the outer segment due to a lack of renewal or to a FAT10-dependent inhibition of PDE6 function could cause visual impairment during inflammation, for example in chorioretinitis or during retinopathies.

Next to its localization, several possibilities for how FAT10 can inhibit PDE6 activity in a noncovalent manner appear imaginable. Structural studies revealed that PDE6 undergoes a conformational change upon activation (14, 16). Therefore, one could speculate that FAT10 blocks this conformational change of PDE6. It was further shown that two transducin α-subunits

binding to the catalytic domain of the catalytic subunits are necessary for PDE6 activation (52). Because FAT10 is binding to the catalytic domain in a covalent and noncovalent manner (Fig. 7), it may block these binding sites. Finally, the cGMP substrate and FAT10 are both binding to the GAFa domain, opening the possibility of competition for binding.

Interestingly, this is another example showing that the noncovalent interaction of FAT10 with a substrate protein has a strong influence on substrate functionality. Whereas the activity of the deconjugating enzyme OTUB1 is enhanced by the interaction with FAT10 (39), the activation of the ubiquitin-like modifier SUMO is blocked when FAT10 interacts with the SUMO E1 activating enzyme AOS1/UBA2 (40). In the present study, FAT10 also had a negative impact on PDE6 activity because noncovalent interaction with FAT10 seemed to inhibit the capability of PDE6 for cGMP hydrolysis (Fig. 7). Overall, these examples imply that FAT10 can have major impacts on substrate proteins other than targeting them to proteasomal degradation.

In summary, we have identified the rod PDE6 as a target protein for FAT10ylation and a noncovalent interaction partner of FAT10 and show that FAT10 down-regulates the protein's activity by guiding PDE6 to proteasomal degradation and by inhibiting its activity. Because PDE6 is a very important protein for the transmission of vision, upcoming studies using different mouse models will help to elucidate the role of FAT10 in more detail and may also open new possibilities for the development of treatment options for certain retinopathies or inflammatory eye diseases that adversely affect vision or even cause blindness.

Experimental procedures

Cell lines, mice, and human tissue

HEK293 cells were originally obtained from ATCC and cultivated in Iscove's modified Dulbecco's Medium (PAN-Biotech) supplemented with 10% FCS (Gibco), 1% stable glutamine (100×, 200 mM; Biowest), and 1% penicillin/streptomycin (100×, PAN-Biotech). Weri-Rb1 cells (ATCC) were cultivated in RPMI 1640 medium (PAN-Biotech) supplemented with 10% FCS (Gibco) and 1% penicillin/streptomycin (100×, PAN-Biotech). The cells were routinely tested to be negative for mycoplasma contamination using the MycoAlert™ Mycoplasma Detection Kit (Lonza).

C57BL/6J mice (H-2b) were originally purchased from Charles River, Germany. Mice were kept in a specific pathogen-free facility at the University of Konstanz, and 6–8-week-old mice were used for all experiments. Sacrifice and organ retrieval was approved by the Review Board of Regierungspräsidium Freiburg.

Human retina tissue was provided by the Moorfields Lions Eye bank (Moorfields Eye Hospital, London, UK), and the study was approved by the Moorfields Biobank Internal Ethics Committee. All of the experiments were undertaken with the understanding and written informed consent of each subject.

Plasmids, cloning, and site-directed mutagenesis

The following plasmids were used for transient transfection of HEK293 cells: pcDNA3.1-His-3xFLAG-FAT10 (30), pcDNA3.1-His-PDE6α (42), pCMV-HA-PDE6β (42), pCMV-

myc-PDE6γ (42), pEGFP-N1-HA-FAT10-GG-GFP (53), pEGFP-N1-HA-FAT10-N-GFP (46), pEGFP-N1-HA-FAT10-C-GFP (46), pCMV6.1-FAT10 (28), and pcDNA3.1-His-3xFLAG-FAT10-AV (34). For generation of pCMV-HA-AIPL1, AIPL1 was amplified by PCR from pCMV-Tag3C-AIPL1 (54) as a template and inserted into pCMV-HA (Clontech) using EcoRI and KpnI as restriction sites. The AIPL1 mutants pCMV-HA-AIPL1-R38C, pCMV-HA-AIPL1-W72S, pCMV-HA-AIPL1-C89R, pCMV-HA-AIPL1-A197P, pCMV-HA-AIPL1-C239R, pCMV-HA-AIPL1-G262S, and pCMV-HA-AIPL1-P376S were generated by site-directed mutagenesis (SDM) of the pCMV-HA-AIPL1 template. For expression of a FLAG-tagged lysine-free FAT10, pcDNA3.1-HA-FAT10 K0 (36) was used as a template for FAT10 PCR amplification. The amplicon was inserted into pcDNA3.1-His-3xFLAG vector via EcoRI and NotI. PDE6β truncation versions expressing either only GAFa or GAFa and GAFb were generated by SDM using pCMV-HA-PDE6β (42) as a template, whereas the PDE catalytic domain was amplified from pCMV-HA-PDE6β and inserted into a pCMV-HA vector via SalI and XhoI. Subsequently, a stop codon was inserted into pCMV-HA-PDE6β PDE directly behind the PDE domain via SDM. For bacterial expression and purification of recombinant HA-tagged AIPL1 proteins, AIPL1 cDNA was amplified from either pCMV-myc-AIPL1, pCMV-myc-AIPL1-A197P, or pCMV-myc-AIPL1-C239R. Amplicons were ligated into a pSUMO vector using BsmBI and HindIII as restriction enzymes. pCMV-myc-AIPL1, pCMV-myc-AIPL1-A197P, pCMV-myc-AIPL1-C239R, and pCMV-FLAG-AIPL1 were cloned by cutting out AIPL1 cDNA from pCMV-HA-AIPL1 or the mutants with restriction enzymes EcoRI and KpnI and subsequent ligation into EcoRI/KpnI-digested pCMV-myc or pCMV-FLAG vector, respectively. FLAG-AIPL1 truncation versions were generated using pCMV-Tag3C-AIPL1-Q163X, pCMV-Tag3C-AIPL1-S328X, pCMV-Tag3C-AIPL1 TPR, and pCMV-Tag3C-AIPL1 TPR + PRD as a template. In brief, pCMV-Tag3C-AIPL1-Q163X and pCMV-Tag3C-AIPL1-S328X were generated by SDM using pCMV-Tag3C-AIPL1 as the template. To construct pCMV-Tag3C-AIPL1 TPR + PRD (AIPL1 169–384) from pCMV-Tag3C-AIPL1, a deletion between amino acid positions 1 and 168 was introduced by SDM. The pCMV-Tag3C-AIPL1 TPR (AIPL1 169–327) construct was generated using pCMV-Tag3C-AIPL1 TPR + PRD as a template and introducing a stop codon by SDM. The respective cDNA was cut out from the template construct with restriction enzymes EcoRI and SalI and subsequently inserted into EcoRI/SalI digested pCMV-FLAG. Untagged AIPL1 and AIPL1-A197P were generated by cutting out AIPL1 cDNA from pCMV-Tag3C-AIPL1 with restriction enzymes EcoRI and KpnI and ligation into EcoRI/KpnI-digested pCMV-FLAG with a C-terminal FLAG tag, thus eliminating expression of the C-terminal FLAG tag due to a stop codon behind AIPL1. The construct pSUMO-myc-PDE6β for bacterial expression and purification of human myc-PDE6β was generated by PCR amplification of PDE6β from pCMV-HA-PDE6β. The myc tag was inserted via the forward primer and the amplicon was ligated into a pSUMO vector using BamHI and XhoI as restriction enzymes. The primer sequences for all constructs are listed in Table S1. All sequences of generated plasmids were verified by sequencing (Microsynth AG).

Induction of endogenous FAT10 expression

The induction of endogenous FAT10 expression was performed as recently described (55). Briefly, HEK293 cells were treated with the pro-inflammatory cytokines TNFα (600 units/ml) and IFN-γ (300 units/ml) (both from PeproTech) for at least 24 h.

Immunoprecipitation and CHX chase experiments

HEK293 cells were transiently transfected with different expression constructs using the TransIT-LTI Transfection Reagent (Mirus Bio). 24 h later, the cells were lysed for 30 min on ice in lysis buffer containing 20 mM Tris/HCl (pH 7.6), 50 mM NaCl, 10 mM MgCl$_2$, and 1% Nonidet P-40, supplemented with 1× protease inhibitor mix (cOmplete™, Mini, EDTA-free Protease Inhibitor mixture, Roche). For cycloheximide (CHX) chase experiments, the cells were treated for indicated time periods with CHX (50 μg/ml final concentration, Sigma-Aldrich), bafilomycin A1 (0.2 μM final concentration, Sigma-Aldrich), chloroquine diphosphate salt (100 μM final concentration, Sigma-Aldrich), or the proteasome inhibitor MG132 (10 μM; Enzo Life Sciences) before harvesting. After taking a sample as loading control, cleared lysates were subjected to immunoprecipitation using either protein A-Sepharose (Sigma-Aldrich) in combination with monoclonal mouse FAT10 antibody clone 4F1 (Enzo Life Sciences) (26), EZview™ Red Anti-FLAG-M2 Affinity Gel (Sigma-Aldrich), anti-HA agarose conjugate HA-7 (Sigma-Aldrich), Anti-FLAG M2 Affinity Gel (Sigma-Aldrich), or EZview™ Red Anti-c-myc Affinity Gel (Sigma-Aldrich). The samples were washed as described before (28), boiled in 5× SDS gel sample buffer containing 4–10% 2-ME, and separated on 4–12% NuPAGE Bis-Tris SDS gradient gels (Invitrogen) or 12.5% Laemmli gels. Western blotting analysis was performed using the respective antibodies: anti-HA–peroxidase (POX) (HA-7), anti-FLAG-HRP (M2), anti-c-myc (9E10), anti-c-myc-POX (9E10), and anti-6-His-POX (His-1) (all Sigma-Aldrich); anti-β-actin (Ac-15), anti-AIPL1 (EPR7711), and anti-GFP (E385) (all Abcam); anti-GST (B-14; Santa Cruz); anti-mouse PDE6β (Thermo Fisher Scientific); anti-FAT10 (4F1; Enzo Life Sciences) (26); anti-ROS-1 (43); anti-FAT10 pAb (36); anti-USE1 (26); anti-mouse IgG2a Isotype Control (Ancell Corporation); and anti-mouse-HRP and anti-rabbit-HRP (both Jackson ImmunoResearch). Immunoblots were visualized using Clarity Western ECL Substrate (Bio-Rad) and the ChemiDoc MP Imaging System (Bio-Rad) with ImageLab 4.1 software. Immunoprecipitation under denaturing conditions was performed as follows: 24 h after transient transfection, confluent HEK293 cells of a 10-cm cell culture dish were washed once with PBS/10 mM N-ethylmaleimide (NEM) and directly lysed with 250 μl of lysis buffer (1× PBS, 2% SDS, 10 mM NEM, 10 mM EDTA, pH 8.0, 10 mM EGTA, pH 8.0, and 1× protease inhibitor (cOmplete™, Mini, EDTA-free Protease Inhibitor mixture, Roche)). In the case of PDE6α and PDE6γ, cells were additionally treated with 10 μM MG132 for 5 h before harvesting. Lysates were sonicated, supplemented with 50 μl 1M DTT, and boiled for 10 min. Renaturation was performed by diluting the boiled samples in 10 volumes of radioimmune precipitation assay buffer (RIPA) (150 mM NaCl, 50 mM Tris-HCl,

pH 8.0, 1% Triton X-100, 0.5% sodium deoxycholate, 0.1% SDS, and 1× protease inhibitor (cOmplete™, Mini, EDTA-free Protease Inhibitor mixture, Roche)), supplemented with 10 mM NEM, 10 mM EDTA, pH 8.0, and 10 mM EGTA, pH 8.0. The lysates were cleared by centrifugation and subjected to immunoprecipitation as described above.

Protein expression and purification

For *in vitro* experiments, recombinant FAT10 variants were expressed and purified as previously described by using pSUMO-FAT10 and pSUMO-FAT10-AV (33, 55).

The construct pDEST17-USE1 (kindly provided by W. Harper) was used to express 6xHis-USE1 (His-USE1) in BL21 (DE3) overnight at 21 °C upon induction of protein expression with 0.4 mM IPTG. Again, bacteria were collected in binding buffer (20 mM Tris, pH 7.5, 150 mM NaCl, 20 mM imidazole, 1 mM tris(2-carboxyethyl)phosphine (TCEP), and 1 tablet/100 ml of protease inhibitor mix (cOmplete™, Mini, EDTA-free Protease Inhibitor mixture, Roche)) and lysed with at least two cycles at 2.5 kbar in a cell disrupter (Constant Cell Disruptor TS, Constant Systems Ltd.). Cleared lysates were loaded onto a preequilibrated 5-ml HisTrap Fast Flow column (GE Healthcare) using AektaExplorer with UNICORN software (both GE Healthcare), and elution was performed with 50% of elution buffer (20 mM Tris-HCl, pH 7.5, 150 mM NaCl, 0.5 M imidazole, and 1 mM TCEP) after washing away unspecifically bound proteins using 5% elution buffer. Subsequent size exclusion chromatography for buffer exchange was performed with a HiPrep 26/10 column (GE Healthcare), and purified protein was stored at −80 °C in desalting/storage buffer containing 20 mM Tris-HCl, pH 7.5, 150 mM NaCl, 1 mM TCEP, and 5% glycerol.

GST was expressed in *Escherichia coli* BL21(DE3) using the pGEX-4T-3 expression construct, and bacteria were grown in modified LB medium at 37 °C to an A_{600} of 0.6. Protein expression was induced for 5 h at 20 °C by the addition of 0.1 mM IPTG. The cells were harvested and lysed as described above, and GST was pulled down for 2 h at 8 °C by using GSH-beads (Sigma-Aldrich). Elution was performed for 30 min at 8 °C in 50 mM Tris, pH 8.0, and supplemented with 5 mM GSH (Fluka). Free GSH was removed using PD10 columns (GE Healthcare) and protein was stored in 50 mM Tris, pH 8.0, at −80 °C. For all purifications of recombinant proteins, purity and concentrations were confirmed by BCA assays (Thermo Fisher Scientific) and Coomassie-stained SDS gels.

For purification of recombinant HA-tagged AIPL1 variants, *E. coli* BL21(DE3) were transformed with expression constructs for the different 6His-SUMO-HA-AIPL1 variants described above and grown at 37 °C in modified LB medium (13.5 g/liter peptone, 7 g/liter yeast extract, 14.9 g/liter glycerol, 2.5 g/liter NaCl, 2.3 g/liter K_2HPO_4, 1.5 g/liter KH_2PO_4, and 0.14 g/liter $MgSO_4 \times 7H_2O$, pH 7.0). Protein expression was induced at 21 °C overnight upon addition of 0.4 mM IPTG. Bacteria were harvested by centrifugation (8000 × *g*, 8 °C, 15 min) and mechanically lysed with at least two cycles at 2.5 kbar in a cell disrupter (Constant Cell Disruptor TS, Constant Systems Ltd.) in binding buffer (20 mM Tris, pH 7.6, 150 mM NaCl, and 20 mM imidazole supplemented with 1× protease inhibitor mix

(cOmplete™, Mini, EDTA-free Protease Inhibitor mixture, Roche). Cleared lysates were used for Nickel pulldown with Ni Superflow60 resin (Takara Bio). His-tagged proteins were eluted by the addition of buffer containing 500 mM imidazole. Buffer exchange for 50 mM Tris-HCl, pH 8.0, and ubiquitin-like-specific protease 1 (Ulp1) digest were performed by dialysis overnight at 8 °C. After removal of the 6His-SUMO tag and His-Ulp1 by Nickel pulldown, HA-tagged AIPL1 variants were applied to size exclusion chromatography using a 16/600 75 column (GE Healthcare). Purified proteins were stored in 50 mM Tris-HCl, pH 8.0, supplemented with 10% glycerol at −80 °C. Protein purity and concentration were confirmed by BCA assays (Thermo Fisher Scientific), dot blots with anti-HA peroxidase-conjugated antibody (Sigma-Aldrich), and colloidal Coomassie-stained SDS gels.

The expression of the pSUMO-myc-PDE6β construct in *E. coli* BL21(DE3) RIPL bacteria was induced with 0.4 mM IPTG at an A_{600} of 0.5–0.7. Bacteria were grown overnight at 21 °C and harvested via centrifugation before cell lysis in 5 ml/g binding buffer (20 mM Tris-HCl, pH 7.5, 150 mM NaCl, 20 mM imidazole, and 1 mM TCEP) using a cell disruptor (Constant Cell Disruptor TS, Constant Systems Ltd.) with at least two cycles at 2.5 kbar. Capture Ni^{2+} affinity chromatography was performed with HisTrap Fast Flow 5-ml columns using the AektaPure system (both GE Healthcare). 6His-SUMO-myc-PDE6β was eluted with elution buffer (20 mM Tris-HCl, pH 7.5, 150 mM NaCl, 500 mM imidazole, and 1 mM TCEP), and the Ulp1 digest was performed overnight at 8 °C after buffer exchange with HiPrep 26/10 desalting columns (GE Healthcare). After a second affinity chromatography with HisTrap Fast Flow 5-ml columns and the AektaPure system (both GE Healthcare), the 6His-SUMO and the Ulp1-6His were separated from myc-PDE6β. The final myc-PDE6β was stored in storage buffer (20 mM Tris-Hcl, pH 7.5, 50 mM NaCl, 10 mM $MgCl_2$, and 1 mM TCEP) at 4 °C and immediately used for the *in vitro* experiments.

In vitro interaction experiments

In vitro interaction assays with HA-tagged recombinant AIPL1 proteins were performed in a final volume of 20 μl of 1× reaction buffer (20 mM Tris-HCl, pH 7.6, 50 mM NaCl, 10 mM $MgCl_2$, and 0.1 mM DTT (all from Sigma-Aldrich), supplemented with 1× protease inhibitor mix (cOmplete™, Mini, EDTA-free Protease Inhibitor mixture; Roche). Recombinant proteins: 4.9 nM FAT10 (1.8 mg/ml), 5.2 nM 6His-ubiquitin (1 mg/ml, Enzo Life Sciences), and 2.7 nM HA-AIPL1 variants (WT 0.5 mg/ml, AIPL1-A197P 0.44 mg/ml, and AIPL1-C239R 0.9 mg/ml) were incubated at 30 °C for 60 min. Because the amounts of HA-tagged AIPL1 proteins could not be determined exactly by calculation, colloidal Coomassie staining of SDS gels was performed for concentration adjustment. After increasing the volume using 1× reaction buffer, immunoprecipitation was performed for 2 h at 4 °C by the addition of anti-HA-agarose conjugate HA-7 (Sigma-Aldrich). In case of ubiquitin, a sample of the supernatant was taken to detect unbound protein. Immunoprecipitation samples were washed twice with NET-TN (50 mM Tris-HCl, pH 8.0, 650 mM NaCl, 5 mM EDTA,

and 0.5% Triton-X-100), twice with NET-T (50 mM Tris-HCl, pH 8.0, 150 mM NaCl, 5 mM EDTA, and 0.5% Triton-X-100) and resuspended in 5× SDS sample buffer containing 4% 2-ME. Proteins were separated on 4–12% NuPAGE Bis-Tris SDS gradient gels (Invitrogen), and Western blotting analysis was performed using the respective antibodies.

In vitro FAT10ylation experiment

The same buffer as for the *in vitro* interaction assays was used, supplemented with 4 mM ATP. The following recombinant proteins were mixed in a final volume of 20 µl: 0.1 nM FLAG-UBA6 (0.56 mg/ml; Enzo Life Sciences), 0.7 nM 6His-USE1 (0.58 mg/ml), 0.013 µM FAT10 (1.6 mg/ml), 0.013 µM FAT10-AV (1.5 mg/ml), and 0.75 nM myc-PDE6β (0.5 µg/µl). The proteins were incubated for 60 min at 30 °C, and the reaction was stopped by the addition of 5× SDS gel sample buffer supplemented with 5% 2-ME. After SDS-PAGE on 4–12% NuPAGE Bis-Tris SDS gradient gels (Invitrogen), Western blotting analysis was performed.

RT-qPCR for human retina samples

Three human retina tissues were provided by the Moorfields Lions Eye Bank (Moorfields Eye Hospital, London, UK). The study was approved by the Moorfields Biobank Internal Ethics Committee. Sex and age characteristics of the donors were as follows: donor 1 (male, 36 years old), donor 2 (female, 37 years old), donor 3 (male, 81 years old). A fourth sample of retina RNA was purchased from Clontech and was described to originate from a Caucasian child. All of the experiments were undertaken with the understanding and written informed consent of each subject, and the study methodologies conformed to the standards set by the Declaration of Helsinki. After removal, retinae were stored in RNA*later* until RNA was extracted using RNeasy Mini Kit (Qiagen) in combination with QIAshredder (Qiagen) according to the manufacturer's protocol. RNA was reverse-transcribed into cDNA using the High-Capacity cDNA Reverse Transcription Kit (Applied Biosystems) according to the manual. As a control, endogenous FAT10 expression was induced by treating HEK293 cells and Weri-Rb1 cells with the pro-inflammatory cytokines TNFα (600 units/ml) and IFN-γ (300 units/ml) (both from Pepro-Tech) for 24 h. Quantitative PCR was performed with the 7900 HT Fast real-time PCR instrument (Applied Biosystems) using primers for human FAT10 (FAT10 fwd: CTGTCTCTG-GTTTCTGGCCC; FAT10 rev: GGAAGCATTGGGAGC-CATCT; (26)), human AIPL1 (Hs_AIPL1_1_SG, Qiagen), UBA6 (Hs_UBA6_1_SG, Qiagen), USE1 (Hs_FLJ13855_1_SG, Qiagen), and GAPDH (Hs_GAPDH_1_SG, Qiagen).

FAT10ylation of mouse PDE6 holoenzyme

Mouse retinae (6 eyes) from 6–8-week-old C57BL/6 (H-2b) WT mice were prepared and lysed in RIPA buffer (150 mM NaCl, 50 mM Tris-HCl, pH 8.0, 1% (v/v) Triton X-100, 0.5% sodium deoxycholate, and 0.1% (w/v) SDS; 500 µl/2 retinae) for 30 min on ice. Additional homogenization was achieved using a 0.7 µm syringe. Retina lysate was pooled and split equally into eight samples. Immunoprecipitation of PDE6 holoenzyme was

performed with protein A-Sepharose in combination with anti-ROS-1 antibody (2.5 µg) overnight at 4 °C. Mouse IgG2a was used as an isotype control. The beads were washed once with NET-TN, once with NET-T, and twice with PBS. The subsequent *in vitro* reaction was executed on top of the beads-bound PDE6 in a final reaction volume of 100 µl of 1× ATP-containing *in vitro* buffer (20 mM Tris-HCl, pH 7.6, 50 mM NaCl, 10 mM MgCl$_2$, 4 mM ATP, and 0.1 mM DTT (all from Sigma-Aldrich), supplemented with 1× protease inhibitor mix (cOmplete^{TM}, Mini, EDTA-free Protease Inhibitor mixture, Roche). Recombinant proteins: 0.05 nM FLAG-UBA6 (0.56 mg/ml; Enzo Life Sciences), 0.3 nM His-USE1 (0.58 mg/ml), 2.62 nM FAT10 (1.6 mg/ml), and 2.75 nM FAT10-AV (0.5 mg/ml) were incubated at 30 °C for 30 min with vigorous shaking. As a control, a sample of the supernatant was taken, boiled in 5× SDS sample buffer, and analyzed by Western blotting under nonreducing conditions. The beads were washed twice with PBS and boiled in 5 × SDS sample buffer supplemented with 4% 2-ME, and proteins were separated under reducing conditions on a 4–12% NuPAGE Bis-Tris SDS gradient gel (Invitrogen). Western blotting analysis was performed using a mouse-specific anti-PDE6β antibody (Thermo Fisher Scientific, PA1-722).

cGMP hydrolysis assay

The activity of mouse PDE6 was measured using the Cyclic Nucleotide Phosphodiesterase Assay Kit (Enzo Life Sciences) according to the manufacturer's instructions. Recombinant Type I cyclic phosphodiesterase included in the kit was used as a positive control. To test mouse PDE6 activity, one retina of a C57BL/6 mouse (H-2b) was prepared and lysed in phosphate-free lysis buffer (50 mM Tris-HCl, pH 7.5, 0.1 mM EDTA, pH 8.0, 0.1 mM EGTA, pH 8.0, 1 mM DTT, and 0.2% Nonidet P-40) for 30 min at 4 °C. Subsequently, lysates were desalted using PD Mini Trap G-25 columns (GE Healthcare) preequilibrated in assay buffer (10 mM Tris-HCl, pH 7.5). Lysates were diluted 1:30 in assay buffer, and a final amount of 5 µl of lysate was used in the assay. Different amounts of FAT10 (1.67 mg/ml, 1.67 µg (+), or 5 µg (++)) or FAT10-AV (1.5 mg/ml) protein (1.5 µg (+) or 4.5 µg (++)) were used as an inhibitor, and FAT10 storage buffer (20 mM Tris-HCl, pH 7.5, 150 mM NaCl, 1 mM TCEP, and 10% glycerol, same volume as the highest FAT10 amount) was used as an additional control. Absorbance measurement at 620 nm was conducted with an Infinity2000 multiplate reader (Tecan). For comparison of retina preparation, 20 µl of each lysate were either analyzed via Western blotting using a specific anti-mouse PDE6β antibody (Thermo Fisher Scientific, PA1-722) or used for a colloidal Coomassie staining with Instant Blue (Expedeon).

Quantification and statistical analysis

For all figures, error bars show mean ± S.E. Densitometric analysis was performed by calculating the respective ECL signal with Image Laboratory4.1 software. Statistical analysis for cGMP hydrolysis assay was performed using one-way analysis of variance with Dunnett correction with GraphPad Prism 6 (GraphPad Software). Differences were considered as

ASBMB

significant for *p* values of $*p < 0.05$, $**p < 0.01$, $***p < 0.001$, and $****p < 0.0001$.

Data availability

All data are contained in this article and in the supporting information.

Abbreviations—The abbreviations used are: 2-ME, β-mercaptoethanol; AIPL1, aryl hydrocarbon interacting protein-like 1; CHX, cycloheximide; FKBP, FK506-binding protein; IPTG, isopropyl-β-d-thio-galactoside; LCA, Leber congenital amaurosis; NEM, *N*-ethylmaleimide; OTUB, otubain; PDE, phosphodiesterase; PRD, proline rich domain; SDM, site-directed mutagenesis; TNF, tumor necrosis factor; TPR, tetratricopeptide repeat; UBA, ubiquitin-like modifier-activating enzyme; UBD, ubiquitin-like domain; UBE, ubiquitin-activating enzyme; USE, UBA6-specific E2-conjugating enzyme; VCP, valosin-containing protein; HLA, human leukocyte antigen; SUMO, small ubiquitin-like modifier; AOS, activation of Smt3p; Co-IP, co-immunoprecipitation; NUB, negative regulator of ubiquitin like proteins; POX, peroxidase; RIPA, radioimmune precipitation assay buffer; TCEP, tris(2-carboxyethyl)phosphine; Ulp, ubiquitin-like-specific protease.

References

1. Baehr, W. (2014) Membrane protein transport in photoreceptors: the function of PDEδ: the Proctor lecture. *Invest. Ophthalmol. Vis. Sci.* **55,** 8653–8666 CrossRef Medline
2. Sung, C. H., and Chuang, J. Z. (2010) The cell biology of vision. *J. Cell Biol.* **190,** 953–963 CrossRef Medline
3. Yadav, R. P., and Artemyev, N. O. (2017) AIPL1: A specialized chaperone for the phototransduction effector. *Cell. Signal.* **40,** 183–189 CrossRef Medline
4. Young, R. W. (1971) The renewal of rod and cone outer segments in the rhesus monkey. *J. Cell Biol.* **49,** 303–318 CrossRef Medline
5. Hidalgo-de-Quintana, J., Evans, R. J., Cheetham, M. E., and van der Spuy, J. (2008) The Leber congenital amaurosis protein AIPL1 functions as part of a chaperone heterocomplex. *Invest. Ophthalmol. Vis. Sci.* **49,** 2878–2887 CrossRef Medline
6. Sohocki, M. M., Bowne, S. J., Sullivan, L. S., Blackshaw, S., Cepko, C. L., Payne, A. M., Bhattacharya, S. S., Khaliq, S., Qasim Mehdi, S., Birch, D. G., Harrison, W. R., Elder, F. F., Heckenlively, J. R., and Daiger, S. P. (2000) Mutations in a new photoreceptor-pineal gene on 17p cause Leber congenital amaurosis. *Nat. Genet.* **24,** 79–83 CrossRef Medline
7. van der Spuy, J., Chapple, J. P., Clark, B. J., Luthert, P. J., Sethi, C. S., and Cheetham, M. E. (2002) The Leber congenital amaurosis gene product AIPL1 is localized exclusively in rod photoreceptors of the adult human retina. *Hum. Mol. Genet.* **11,** 823–831 CrossRef Medline
8. van der Spuy, J., Kim, J. H., Yu, Y. S., Szel, A., Luthert, P. J., Clark, B. J., and Cheetham, M. E. (2003) The expression of the Leber congenital amaurosis protein AIPL1 coincides with rod and cone photoreceptor development. *Invest. Ophthalmol. Vis. Sci.* **44,** 5396–5403 CrossRef Medline
9. Sacristan-Reviriego, A., and van der Spuy, J. (2018) The Leber congenital amaurosis-linked protein AIPL1 and Its critical role in photoreceptors. *Adv. Exp. Med. Biol.* **1074,** 381–386 CrossRef Medline
10. Kolandaivelu, S., Huang, J., Hurley, J. B., and Ramamurthy, V. (2009) AIPL1, a protein associated with childhood blindness, interacts with α-subunit of rod phosphodiesterase (PDE6) and is essential for its proper assembly. *J. Biol. Chem.* **284,** 30853–30861 CrossRef Medline
11. Baehr, W., Devlin, M. J., and Applebury, M. L. (1979) Isolation and characterization of cGMP phosphodiesterase from bovine rod outer segments. *J. Biol. Chem.* **254,** 11669–11677 Medline
12. Deterre, P., Bigay, J., Forquet, F., Robert, M., and Chabre, M. (1988) cGMP phosphodiesterase of retinal rods is regulated by two inhibitory subunits. *Proc. Natl. Acad. Sci. U.S.A.* **85,** 2424–2428 CrossRef Medline
13. Gillespie, P. G., and Beavo, J. A. (1988) Characterization of a bovine cone photoreceptor phosphodiesterase purified by cyclic GMP-Sepharose chromatography. *J. Biol. Chem.* **263,** 8133–8141 Medline
14. Gulati, S., Palczewski, K., Engel, A., Stahlberg, H., and Kovacik, L. (2019) Cryo-EM structure of phosphodiesterase 6 reveals insights into the allosteric regulation of type I phosphodiesterases. *Sci. Adv.* **5,** eaav4322 CrossRef Medline
15. Muradov, H., Boyd, K. K., and Artemyev, N. O. (2004) Structural determinants of the PDE6 GAF A domain for binding the inhibitory γ-subunit and noncatalytic cGMP. *Vision Res.* **44,** 2437–2444 CrossRef Medline
16. Zhang, Z., He, F., Constantine, R., Baker, M. L., Baehr, W., Schmid, M. F., Wensel, T. G., and Agosto, M. A. (2015) Domain organization and conformational plasticity of the G protein effector, PDE6. *J. Biol. Chem.* **290,** 12833–12843 CrossRef Medline
17. Cote, R. H. (2004) Characteristics of photoreceptor PDE (PDE6): similarities and differences to PDE5. *Int. J. Impot. Res.* **16,** S28–33 CrossRef Medline
18. Zhang, X., and Cote, R. H. (2005) cGMP signaling in vertebrate retinal photoreceptor cells. *Front. Biosci.* **10,** 1191–1204 CrossRef Medline
19. Anant, J. S., Ong, O. C., Xie, H. Y., Clarke, S., O'Brien, P. J., and Fung, B. K. (1992) *In vivo* differential prenylation of retinal cyclic GMP phosphodiesterase catalytic subunits. *J. Biol. Chem.* **267,** 687–690 Medline
20. Cheguru, P., Zhang, Z., and Artemyev, N. O. (2014) The GAFa domain of phosphodiesterase-6 contains a rod outer segment localization signal. *J. Neurochem.* **129,** 256–263 CrossRef Medline
21. Bett, J. S., Kanuga, N., Richet, E., Schmidtke, G., Groettrup, M., Cheetham, M. E., and van der Spuy, J. (2012) The inherited blindness protein AIPL1 regulates the ubiquitin-like FAT10 pathway. *PLoS ONE* **7,** e30866 CrossRef Medline
22. Bates, E. E., Ravel, O., Dieu, M. C., Ho, S., Guret, C., Bridon, J. M., Ait-Yahia, S., Brière, F., Caux, C., Banchereau, J., and Lebecque, S. (1997) Identification and analysis of a novel member of the ubiquitin family expressed in dendritic cells and mature B cells. *Eur. J. Immunol.* **27,** 2471–2477 CrossRef Medline
23. Buerger, S., Herrmann, V. L., Mundt, S., Trautwein, N., Groettrup, M., and Basler, M. (2015) The Ubiquitin-like modifier FAT10 is selectively expressed in medullary thymic epithelial cells and modifies T cell selection. *J. Immunol.* **195,** 4106–4116 CrossRef Medline

ASBMB

J. Biol. Chem. (2020) 295(42) 14402–14418 **14417**

24. Canaan, A., Yu, X., Booth, C. J., Lian, J., Lazar, I., Gamfi, S. L., Castille, K., Kohya, N., Nakayama, Y., Liu, Y. C., Eynon, E., Flavell, R., and Weissman, S. M. (2006) FAT10/diubiquitin-like protein-deficient mice exhibit minimal phenotypic differences. *Mol. Cell Biol.* **26,** 5180–5189 CrossRef Medline

25. Lukasiak, S., Schiller, C., Oehlschlaeger, P., Schmidtke, G., Krause, P., Legler, D. F., Autschbach, F., Schirmacher, P., Breuhahn, K., and Groettrup, M. (2008) Proinflammatory cytokines cause FAT10 upregulation in cancers of liver and colon. *Oncogene* **27,** 6068–6074 CrossRef Medline

26. Aichem, A., Pelzer, C., Lukasiak, S., Kalveram, B., Sheppard, P. W., Rani, N., Schmidtke, G., and Groettrup, M. (2010) USE1 is a bispecific conjugating enzyme for ubiquitin and FAT10, which FAT10ylates itself in cis. *Nat. Commun.* **1,** 13 CrossRef Medline

27. Raasi, S., Schmidtke, G., de Giuli, R., and Groettrup, M. (1999) A ubiquitin-like protein which is synergistically inducible by interferon-γ and tumor necrosis factor-α. *Eur. J. Immunol.* **29,** 4030–4036 CrossRef Medline

28. Aichem, A., Anders, S., Catone, N., Rößler, P., Stotz, S., Berg, A., Schwab, R., Scheuermann, S., Bialas, J., Schütz-Stoffregen, M. C., Schmidtke, G., Peter, C., Groettrup, M., and Wiesner, S. (2018) The structure of the ubiquitin-like modifier FAT10 reveals an alternative targeting mechanism for proteasomal degradation. *Nat. Commun.* **9,** 4646 CrossRef Medline

29. Groettrup, M., Pelzer, C., Schmidtke, G., and Hofmann, K. (2008) Activating the ubiquitin family: UBA6 challenges the field. *Trends Biochem. Sci.* **33,** 230–237 CrossRef Medline

30. Chiu, Y. H., Sun, Q., and Chen, Z. J. (2007) E1-L2 activates both ubiquitin and FAT10. *Mol. Cell* **27,** 1014–1023 CrossRef Medline

31. Jin, J., Li, X., Gygi, S. P., and Harper, J. W. (2007) Dual E1 activation systems for ubiquitin differentially regulate E2 enzyme charging. *Nature* **447,** 1135–1138 CrossRef Medline

32. Pelzer, C., Kassner, I., Matentzoglu, K., Singh, R. K., Wollscheid, H. P., Scheffner, M., Schmidtke, G., and Groettrup, M. (2007) UBE1L2, a novel E1 enzyme specific for ubiquitin. *J. Biol. Chem.* **282,** 23010–23014 CrossRef Medline

33. Aichem, A., Catone, N., and Groettrup, M. (2014) Investigations into the auto-FAT10ylation of the bispecific E2 conjugating enzyme UBA6-specific E2 enzyme 1. *FEBS J.* **281,** 1848–1859 CrossRef Medline

34. Aichem, A., Kalveram, B., Spinnenhirn, V., Kluge, K., Catone, N., Johansen, T., and Groettrup, M. (2012) The proteomic analysis of endogenous FAT10 substrates identifies p62/SQSTM1 as a substrate of FAT10ylation. *J. Cell Sci.* **125,** 4576–4585 CrossRef Medline

35. Bialas, J., Groettrup, M., and Aichem, A. (2015) Conjugation of the ubiquitin activating enzyme UBE1 with the ubiquitin-like modifier FAT10 targets it for proteasomal degradation. *PLoS ONE* **10,** e0120329 CrossRef Medline

36. Hipp, M. S., Kalveram, B., Raasi, S., Groettrup, M., and Schmidtke, G. (2005) FAT10, a ubiquitin-independent signal for proteasomal degradation. *Mol. Cell Biol.* **25,** 3483–3491 CrossRef Medline

37. Rani, N., Aichem, A., Schmidtke, G., Kreft, S. G., and Groettrup, M. (2012) FAT10 and NUB1L bind to the VWA domain of Rpn10 and Rpn1 to enable proteasome-mediated proteolysis. *Nat. Commun.* **3,** 749 CrossRef Medline

38. Schmidtke, G., Aichem, A., and Groettrup, M. (2014) FAT10ylation as a signal for proteasomal degradation. *Biochim. Biophys. Acta* **1843,** 97–102 CrossRef Medline

39. Bialas, J., Boehm, A. N., Catone, N., Aichem, A., and Groettrup, M. (2019) The ubiquitin-like modifier FAT10 stimulates the activity of the deubiquitylating enzyme OTUB1. *J. Biol. Chem.*

40. Aichem, A., Sailer, C., Ryu, S., Catone, N., Stankovic-Valentin, N., Schmidtke, G., Melchior, F., Stengel, F., and Groettrup, M. (2019) The ubiquitin-like modifier FAT10 interferes with SUMO activation. *Nat. Commun.* **10,** 4452 CrossRef Medline

41. Zeytuni, N., and Zarivach, R. (2012) Structural and functional discussion of the tetra-trico-peptide repeat, a protein interaction module. *Structure* **20,** 397–405 CrossRef Medline

42. Sacristan-Reviriego, A., Bellingham, J., Prodromou, C., Boehm, A. N., Aichem, A., Kumaran, N., Bainbridge, J., Michaelides, M., and van der Spuy, J. (2017) The integrity and organization of the human AIPL1 functional domains is critical for its role as a HSP90-dependent co-chaperone for rod PDE6. *Hum. Mol. Genet.* **26,** 4465–4480 CrossRef Medline

43. Hurwitz, R. L., and Beavo, J. A. (1984) Immunotitration analysis of the rod outer segment phosphodiesterase. *Adv. Cyclic Nucleotide Protein Phosphorylation Res.* **17,** 239–248 Medline

44. Mou, H., and Cote, R. H. (2001) The catalytic and GAF domains of the rod cGMP phosphodiesterase (PDE6) heterodimer are regulated by distinct regions of its inhibitory γ subunit. *J. Biol. Chem.* **276,** 27527–27534 CrossRef Medline

45. Ramamurthy, V., Niemi, G. A., Reh, T. A., and Hurley, J. B. (2004) Leber congenital amaurosis linked to AIPL1: a mouse model reveals destabilization of cGMP phosphodiesterase. *Proc. Natl. Acad. Sci. U.S.A.* **101,** 13897–13902 CrossRef Medline

46. Schmidtke, G., Kalveram, B., Weber, E., Bochtler, P., Lukasiak, S., Hipp, M. S., and Groettrup, M. (2006) The UBA domains of NUB1L are required for binding but not for accelerated degradation of the ubiquitin-like modifier FAT10. *J. Biol. Chem.* **281,** 20045–20054 CrossRef Medline

47. Kanaya, K., Sohocki, M. M., and Kamitani, T. (2004) Abolished interaction of NUB1 with mutant AIPL1 involved in Leber congenital amaurosis. *Biochem. Biophys. Res. Commun.* **317,** 768–773 CrossRef Medline

48. Martínez-Fernández de la Cámara, C., Sequedo, M. D., Gómez-Pinedo, U., Jaijo, T., Aller, E., García-Tárraga, P., García-Verdugo, J. M., Millán, J. M., and Rodrigo, R. (2013) Phosphodiesterase inhibition induces retinal degeneration, oxidative stress and inflammation in cone-enriched cultures of porcine retina. *Exp. Eye Res.* **111,** 122–133 CrossRef Medline

49. Choi, Y., Kim, J. K., and Yoo, J. Y. (2014) NFκB and STAT3 synergistically activate the expression of FAT10, a gene counteracting the tumor suppressor p53. *Mol. Oncol.* **8,** 642–655 CrossRef Medline

50. Schmidtke, G., Kalveram, B., and Groettrup, M. (2009) Degradation of FAT10 by the 26S proteasome is independent of ubiquitylation but relies on NUB1L. *FEBS Lett.* **583,** 591–594 CrossRef Medline

51. Keravis, T., and Lugnier, C. (2012) Cyclic nucleotide phosphodiesterase (PDE) isozymes as targets of the intracellular signalling network: benefits of PDE inhibitors in various diseases and perspectives for future therapeutic developments. *Br. J. Pharmacol.* **165,** 1288–1305 CrossRef Medline

52. Irwin, M. J., Gupta, R., Gao, X. Z., Cahill, K. B., Chu, F., and Cote, R. H. (2019) The molecular architecture of photoreceptor phosphodiesterase 6 (PDE6) with activated G protein elucidates the mechanism of visual excitation. *J. Biol. Chem.*

53. Hipp, M. S., Raasi, S., Groettrup, M., and Schmidtke, G. (2004) NEDD8 ultimate buster-1L interacts with the ubiquitin-like protein FAT10 and accelerates its degradation. *J. Biol. Chem.* **279,** 16503–16510 CrossRef Medline

54. van der Spuy, J., and Cheetham, M. E. (2004) The Leber congenital amaurosis protein AIPL1 modulates the nuclear translocation of NUB1 and suppresses inclusion formation by NUB1 fragments. *J. Biol. Chem.* **279,** 48038–48047 CrossRef Medline

55. Aichem, A., Boehm, A. N., Catone, N., Schmidtke, G., and Groettrup, M. (2019) Analysis of modification and proteolytic targeting by the ubiquitin-like modifier FAT10. *Methods Enzymol.* **618,** 229–256 CrossRef Medline